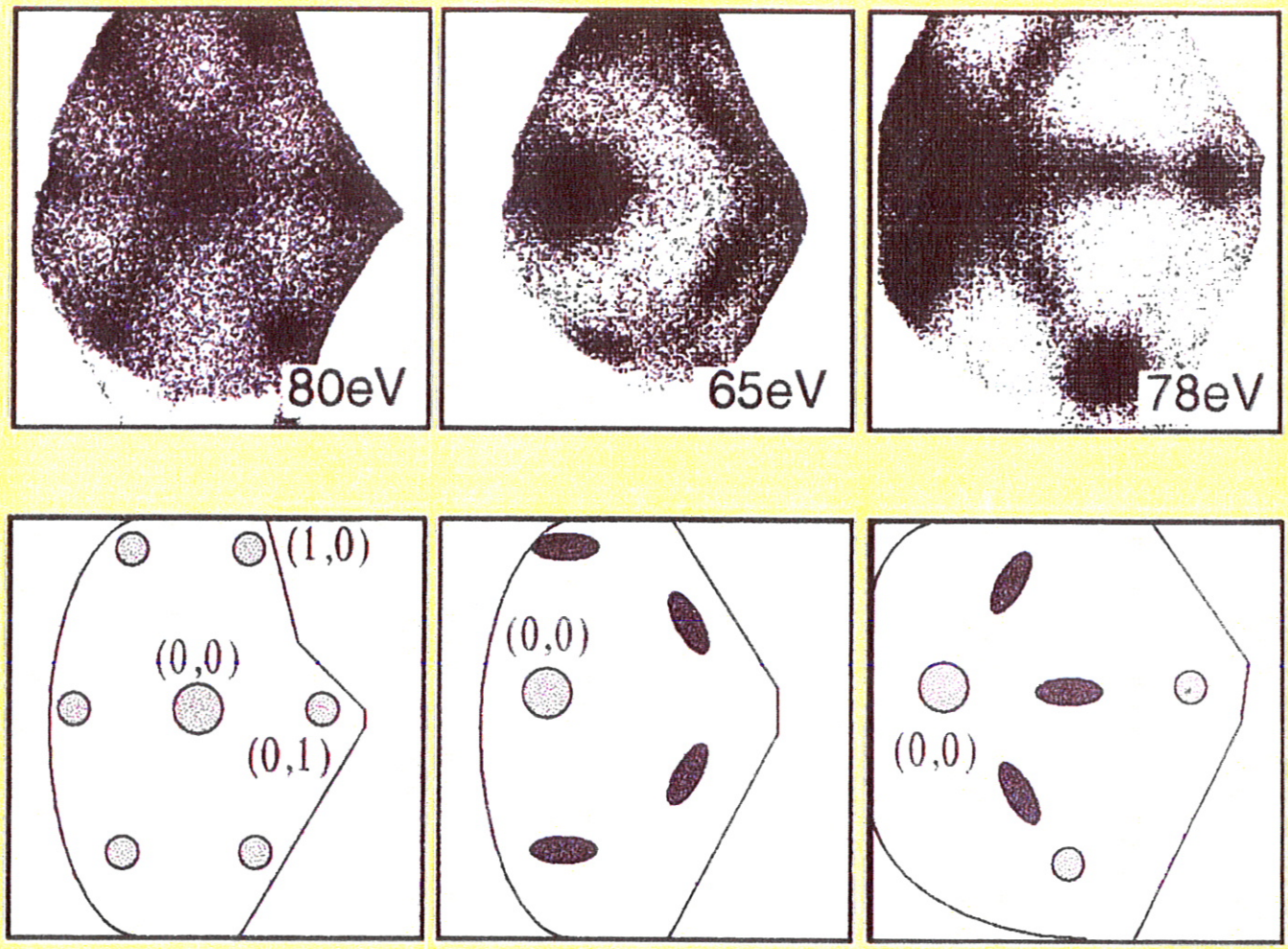


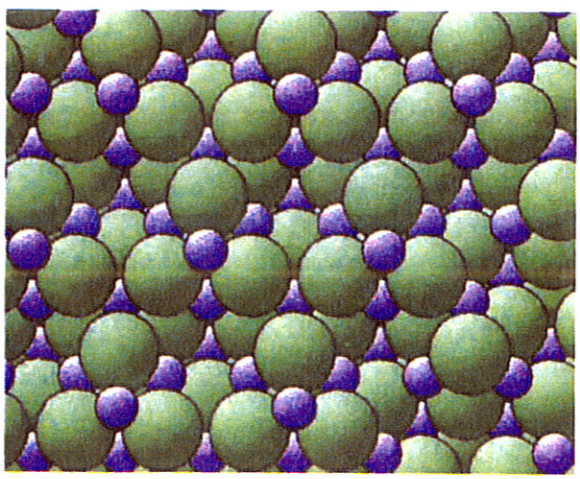

Octopolar reconstruction of an NiO(111) film on an Ni(111) surface is clearly evident from electron diffraction and electron energy loss spectroscopy (dark ellipses: superstructure reflections; light grey shaded circles: main structure reflections), and is modeled as shown on the left.

# Adsorption of Gases on Complex Solid Surfaces

Hans-Joachim Freund*

*Dedicated to Professor Gerhard Ertl on the occasion of his 60th birthday*

During the last thirty years the research field of surface science with its various disciplines has progressively played a more and more important role in the field of catalysis. The main focus of attention for a long time was research on metal surfaces, on which, in time, the whole spectrum of developed surface analytical methods was applied. This led to a better understanding of the mechanisms of catalytic reactions, such as the synthesis of ammonia and the oxidation of CO, especially through the work of Gerhard Ertl.[1, 2] In contrast to clean metal surfaces, surfaces of real catalysts are complex entities, the structures of which can have a strong influence on the processes occurring on the surface. Thus, it seems logical to employ the typical structural characteristics and the morphology of the catalytic surface as guidelines in the investigation of complex model systems. In this review the preparation, and structural and electronic characterization of such model systems will be discussed. Clean surfaces of catalytically active oxides, as well as model systems for dispersed transition metal/support catalysts will be characterized in terms of their morphology and electronic structure as well as their adsorption and reaction capabilities.

**Keywords:** adsorption · heterogeneous catalysis · surface analysis · surface chemistry

## 1. Introduction

Surfaces of solid materials are interesting research objects.[3] Nowadays, a detailed knowledge of the correlation between geometric and electronic structure and their effects on chemical reactivity is already available for certain classes of materials such as metals and elemental semiconductors.[4] In contrast, corresponding information for many, very simple compound systems such as oxides, carbides, and nitrides is still very rudimentary.[5, 6] This is even more surprising, since a great number of compound systems show technically relevant reactivities on surfaces, and oxides are suitable support materials for dispersed metal catalysts. In such cases, there are distinct interactions between metal and oxide such that the complex structural and electronic processes on the interface between metal and support determine the chemical reactivity. Presumably these are the reasons for the recently increased activity in this area.[5–15] In their book *Surface Science of Oxide Surfaces* Henrich and Cox impressively summarized the data known up to the beginning of the 1990s on the clean substrate.[6] It is clear that for experiments on oxide surfaces, a typical example of a compound surface, the preparation of the sample plays a significant role: from the thermodynamic point of view, a well-defined oxygen pressure in the gas phase determines the oxide stoichiometry.[18] This does not exist under ultrahigh vacuum (UHV) conditions necessary for surface experiments. The stoichiometry of the material under these conditions is, thus, sometimes determined only by a kinetic hindrance, and therefore the method of sample preparation is of significant importance. The methods of preparation of the surface give rise to essentially two categories of experiments on compound surfaces: 1. Experiments on surfaces on single crystals;[5] 2. experiments on epitaxially grown thin films.[7]

Whereas, in research on thin films one must always consider whether the electronic structure of the substrate corresponds to that of the single crystal, this problem naturally does not occur for samples of the first catergory. However, experimental difficulties associated with the execution and interpretation of electronic spectroscopic measurements can occur (charging etc.) when dealing with an electrical insulator as a single crystal. Also rapid heating and cooling of the surface of the sample can be a problem in such cases. In thin film studies these problems are limited by the thickness of the film, from which it is possible to determine if the electronic structure of the film is comparable to that of a single crystal. Furthermore, different crystallographic orientations in the form of thinly covered surfaces can be successfully prepared. This can be a distinct advantage over the use of single crystals when considering experiments on polar surfaces of ionic solids. This question will be dealt with in more detail in Section 3.1.

[*] Prof. Dr. H.-J. Freund
Fritz-Haber-Institut der Max-Planck-Gesellschaft
Faradayweg 4-6, D-14195 Berlin (Germany)
Fax: Int. code +(30)84134101
e-mail: freund@fhi-berlin.mpg.de

The comprehensive study of compound surfaces would certainly benefit from a combination of both strategies. It appears highly likely that in the future experiments will provide similarly detailed information about compound surfaces as is known about metal surfaces.[3] With the increasing knowledge about compound surfaces, such as oxides, it becomes more tempting to go a step further in terms of the complexity of the system and move towards modeling dispersed metal catalysts.[19] Hereby we could possibility benefit from the combination of the above-mentioned research directions and to a certain extent form a bridge to application. In this area the experience gained with metal surfaces and compound surfaces can be combined. To fulfill the modeling of dispersed model catalysts metals would be introduced onto the appropriate compound surfaces (e.g. oxide surfaces).[20] Some examples will be discussed in this review, though not only in terms of the structure and morphology of these systems but also in terms of their electronic structure, their adsorption properties, and their chemical reactivity.

Thus, in light of these considerations we include a section on clean oxide surfaces followed by one about dispersed metal systems on oxide supports; however, first of all in the next section we introduce the terms applied and list the techniques utilized.

## 2. Terms and Techniques

If one splits a regular lattice along one of the crystallographic directions, two sublattices are formed that both have regular surfaces as boundaries. With elementary solids these surfaces are identical; however, this is not necessarily the case for compounds. The resulting surfaces are termed volume-terminated. The surface atoms are located at a different coordination environment than the atoms in the bulk. This leads to a change of the interatomic distances and manifests itself, for example, through the relaxation of the interlayer distances or in a reconstruction; that is, a full lateral and vertical (buckling) restructuring of the atoms in the surface and in the regions near to the surface.

The structures are frequently characterized by electron diffraction (low energy electron diffraction (LEED)) or by imaging procedures (scanning tunneling microscopy (STM), atomic force microscopy (AFM)), and the surface lattice is characterized in terms of lattice vectors in units of length and with respect to the orientation of the bulk lattice vectors.[21, 22] Figure 1 (for an extensive discussion see Section 3.1) shows situations in which both the lateral order of the atoms and the interlayer distances have changed. The lattice vectors of the surface unit cell are twice as long as those in the bulk and are oriented in exactly the same way. This is referred to as a $p(2 \times 2)$ structure (p = primitive, $(2 \times 2)$ = double length in both directions of the surface). Correspondingly, $(\sqrt{3} \times \sqrt{3})R30^\circ$ denotes a structure with crystal vectors, which are $\sqrt{3}$ times longer than that of the

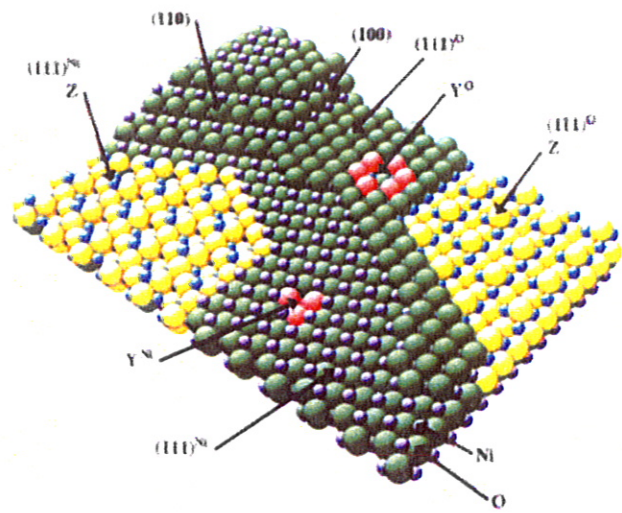


Figure 1. Possible defects in a predominantly (111)-orientated NiO surface. The ideal (111) surfaces could occur as oxygen- or nickel-terminated. Furthermore, facets could exist with (110) or (100) orientation next to point defects Y and octopolar reconstructed regions Z. The reconstructed surface can be both nickel- and oxygen-terminated.

*Hans-Joachim Freund, born in 1951, studied physics and chemistry at the Universität Köln as a fellow of the Studienstiftung des Deutschen Volkes and received his doctorate in 1978 under the supervision of G. Hohlneicher, for a thesis on quantum chemical calculations and spectroscopic studies on transition metal carbonyl compounds in comparison with CO adsorbates. Between 1979 and 1981 he worked in the group of E. W. Plummer in the Physics Department at the University of Pennsylvania on synchrotron studies of the electronic structure of adsorbates. After his return to Köln he recieved a venia legendi in chemical physics in 1983, and in the same year accepted a position as associate professor at the Institut für Physikalische und Theoretische Chemie der Universität Erlangen-Nürnberg. There he worked on $CO_2$ and $N_2$ activation. In 1987 he accepted a position as full professor for physical chemistry at the Ruhr-Universität Bochum, where he founded and until 1995 headed a DFG research group on model catalysts. After not following further offers for chairs in physical chemistry at other universities, he accepted a position as scientific member and director at the Fritz-Haber Institut der Max-Planck-Gesellschaft in Berlin, where he now heads the Department of Chemical Physics. In 1995 he received the Gottfried Wilhelm Leibniz Award of the Deutsche Forschungsgemeinschaft, and since 1996 he is an ordinary member of the Chemical Sciences Section of the Academia Europaea. He is a member of several scientific societies and has published more than 200 scientific papers.*

bulk and which are both rotated by 30° anticlockwise with respect to the bulk lattice vectors (R30°).

In order to determine the interatomic distances and atom coordination experimentally, in the electron diffraction experiment a definite geometry is chosen, and the wavelength of the scattered electrons is varied simply through a change in the acceleration voltage $V$. The number of diffracted electrons in a certain reflection, that is the current $I$, is then determined as a function of $V$. Thereby $I/V$ curves are obtained, which are fitted through model calculations for structure determination.[22] The system is stabilized by surface reconstructions and adopts the corresponding minimal surface energy.[23]

Surface defects and inhomogeneities play a special role in the stability of the surface. Defects can be characterized with respect to their structure and distribution by analysis of the reflection profiles in electron diffraction patterns. In order to eliminate the influence of the surroundings such that clean surfaces can be investigated, the surfaces are prepared under ultrahigh vacuum conditions of between $10^{-8}$ and $10^{-9}$ Pa, under which only a comparitively small number of collisions per centimeter squared of surface is expected in about an hour. If a "clean" surface is placed in a gas atmosphere, the surface atoms in regular sites and defects are capable of bonding through their unfilled valencies to atoms or molecules from the gas phase, and thus stabilize the surface.

The surface structures adopted after gas adsorption clearly are generally different from those of the clean surfaces. The lattice vectors are characterized as discussed above. Evidently, the structures formed depend on the amount of gas adsorbed. Since the actual amount of gas bound is determined by the sticking probability, frequently no absolute surface coverage is given, but only the gas dosage. The unit of the dosage is the Langmuir (L) and corresponds to a supply of a gas at $10^{-4}$ Pa for 1 s. This unit became established because at this dosage it was possible to obtain full coverage with a sticking probability of 1 on a surface of 1 $cm^2$ in 1 s.

Even though absolute coverages are not usually indicated, they can be determined experimentally.[24] A typical procedure is based on thermal desorption spectroscopy (TDS), in which the flow of the desorbed particles from the surface is determined with a quadrupole mass spectrometer, while the temperature of the sample is continually increased. Kinetic parameters such as the activation energy for the desorption and the desorption rate and order can be determined from the form and temperature range of the observed desorption structures. Thermodynamic data are accessible by analyzing the adsorption isotherms. Calorimetric measurements are likewise possible.

PES: photoelectron spectroscopy
XPS: X-ray photoelectron spectroscopy
(AR)UPS: (angle-resolved) ultraviolet photoelectron spectroscopy
AES: Auger electron spectroscopy
(HR)EELS: (high-resolution) electron energy loss spectroscopy
HAS: helium ion scattering
ISS: ion-scattering spectroscopy
STM: scanning tunneling microscopy
AFM: atomic force microscopy
(SPA)-LEED:(spot profile analysis) low-energy electron diffraction
IRAS: infrared reflection absorption spectroscopy

Scheme 1. Surface-sensitive spectroscopic procedures.

The spectroscopic properties are established by a number of surface-sensitive procedures. Scheme 1 contains acronyms and procedures, which are frequently applied. The methods have been discussed in detail in the literature.[4, 21–24] A final comment: the reason for the use of electron spectroscopic procedures is based on the strong interaction between electrons and the condensed state. This limits the escape depth of the electrons from the solid and causes the high surface sensitivity of the procedures.

## 3. Experiments on Clean Oxide Surfaces

### 3.1. Structural Principles and Energetics

Systems that crystallize in a simple lattice type are particularly well suited to introducing structural principles and energetics of compound systems.[6] These systems include binary oxides that exhibit a rock salt lattice, that is NiO,[23] CoO,[24] FeO.[25] Figure 1 shows a schematic representation of the NiO surface[25] with differently oriented facets. The corresponding surface energies are given in Table 1. The following discussion will show that the greatly differing energies, which will be considered in detail, fundamentally determine the reaction behavior.

Table 1. Surface energies in the NiO system.

| Surface | $E_{OF}$ [J m$^{-2}$] |
|---|---|
| NiO(100) | 1.74 [29] |
| NiO(110) | 3.98 [29] |
| NiO(111) | $\infty$ [29] |
| NiO(111) missing row | 8.18 [30] |
| NiO(111) octopolar | 4.28 [30] |
| NiO(111) hydroxylated | not known, but possibly $< E_{OF}$(110) [32] |

Starting from the nonpolar (100) surface, the surface potential will be discussed with the aid of the stacking sequence along the normal of the surface[26] as shown in Figure 2. Thereby we will start with the extreme case of full ionic bonding; that is the covalent share of the bonding and of the hybridization will be initially neglected. On a nonpolar surface there are equal numbers of cations and anions available. This is not only valid for the surface but also for every layer along the {001} direction. This results in a disappearing dipole moment $\mu$ perpendicular to the surface, regardless of the number of stacked layers. The potential has its final value directly on the surface and drops exponentially in vacuum.

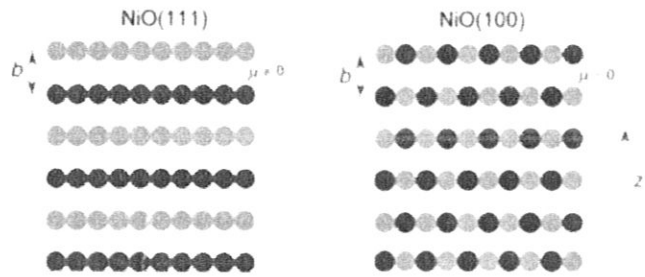


Figure 2. Charge distribution in polar (left) and nonpolar (right) oxide surfaces. Section perpendicular to surface. $b$ = interatomic distance.

In contrast, a completely different situation exists on polar surfaces. Every layer is occupied with only one sort of ion, and consequently, because of the stoichiometry, a transition to the next layer results in a change in the type of ion and charge. Thus, there is a dipole moment perpendicular to the surface that increases linearly with the number of layers $N$ and diverges with $N$ tending to infinity. In the simplest case of a completely ionic bond the potential $V$ at the surface can be described with Equation (a).[27] The potential disappears only very slowly into the vacuum with clear expansion of the surface ($S$: size of the surface unit cell).

$$V = \frac{2\pi}{S}[\mathrm{Nb}(2\sigma - 1) + b(1 - \sigma)] \qquad \text{(a)}$$

Such a situation leads to unstable surfaces, which as a rule cannot be produced to a high standard through cleavage of a single crystal. The corresponding attempts led to strongly faceted surfaces, in which the facet faces again consist of the stable, nonpolar layers with the characteristic coordination of the ions. A coordination like that of the polar surface is found only at the corners and tips of the faceted areas.[5, 28, 29]

Concepts of how such an unstable situation can be stabilized can be derived from Equation (a): Since $\sigma$ represents the charge on the surface relative to a reference layer in the center of the crystal, it shows clearly that the surface charge reduces to half its value ($\sigma = 1/2$) through the disappearance of the linear divergence terms in $N$. This layer charge reduction can be achieved in several ways:

a) by the loss of ions from the first layer of the surface[30]
b) by a reconstruction of the surface affecting several layers[28, 29]
c) by a terracing with long-range periodicity
d) by providing the surface with an adsorbed layer with only half the charge.[31]

Figure 3 shows schematically how these charge reductions alter the surface structure. In Figure 3a half of all ions in rows in the first layer have been arbitrarily removed. Since on a hexagonal surface there are three equivalent directions, a domain structure can be expected with an electron diffraction pattern corresponding to a p(2 × 2) structure. Figure 3b shows a reconstruction extending over several layers, which has already been discussed very early on by Lacman[28] as a possible stabilization of the polar rock salt surface. Recently Wolf[29] showed theoretically that this is in fact the most stable reconstruction (see also Table 1).[32] This kind of surface reconstruction is described as an octopolar reconstruction because it can be identified by octopolar cube units in the surface. This reconstruction can also be regarded as a faceting with (100) microfacets. A more detailed examination allows us to recognize the concept of charge reduction.[6] Concentrating on the first layer, three-quarters of the cations are missing, which corresponds to a charge reduction of 75%, which is correspondingly 50% more than the condition required for stability (i.e. 50% charge reduction). In contrast, in the second, negatively charged layer, only a quarter of the corresponding counterions are missing, thus 50% less than the requirements for stability. The third layer is already complete. In summary, the first and second layers give an overrall charge reduction of 50%. This reduction would lead to a hexagonal structure likewise with a p(2 × 2) electron diffraction pattern.

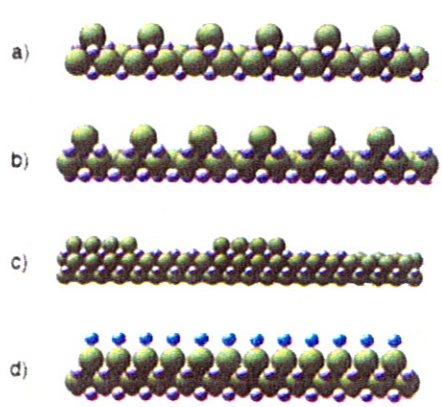


Figure 3. Possibilities for stabilizing polar surfaces: a) Charge reduction by removal of half of the $O^{2-}$ ions, b) octopolar reconstruction, c) domain formation, d) adsorption.

Figure 3c depicts a terracing, which involves the first to third layers and leads on average to a halving of the charge on the surface. However, one must not forget that above every single terrace the surface potential diverges, and only on average is the condition for stability fulfilled. Thus, it is assumed that if such a situation occurs, the size of the terraces must be very limited. The diffraction pattern relative to that obtained in the reconstruction case would not be changed to a first approximation. Figure 3d shows the adsorbate termination of the polar surface. In exact terms, this could be imagined as a layer of $OH^-$ ions, which would have only half the charge of a pure $O^{2-}$ ion layer. The formation would occur either through the adsorption of protons on an oxygen-terminated layer or through adsorption of $OH^-$ ions on a nickel-terminated layer.[31] The electron diffraction pattern would not be differentiated from the nonreconstructed layer with respect to the symmetry. However, the changed electron diffraction cross sections would be revealed experimentally from the current–voltage curves.

Nonpolar and polar surfaces can be prepared experimentally in different ways.[7–17] The techniques have been described often and thus shall not be discussed in detail here. In summary there are three techniques: In the first, the single crystal is cleaved in situ under UHV conditions and investigated.[5] In the second method the single crystal is cut under non-UHV conditions and then under UHV conditions cleaned and prepared through sputtering, and finally heated in an oxygen atmosphere.[5, 12–16] The third method involves the production of thin films through epitaxial growth.[7] The advantages and disadvantages of the different kinds of sample were indicated in the introduction.

### 3.2. Adsorption and Reactivity: Nonpolar Surfaces

Nonpolar surfaces show, when perfectly prepared, increasingly low adsorption enthalpies. In conjunction with this the surface loses chemical reactivity. In all documented experiments the perfect terraces are very similar to a bulk-terminated surface. LEED experiments[33–38] and increasingly also He diffraction studies[39, 40] show only small relaxations and a slight "buckling" of the first layer with outward relaxation of the large

anions. The effects are all within the range of a few percent of the interlayer distances and will not be described in detail here. In the ideal case of perfect terraces, molecules such as NO and CO are relatively weakly bound to the nonpolar surface. CO/MgO(100) has an adsorption energy of 0.2 eV and represents a physisorbed system.[41-43] CO/NiO(100)[44] and NO/NiO[22] display adsorption energies of 0.3 and 0.5 eV, respectively, somewhat stronger interactions, which one would describe as strong physisorption or very weak chemisorption. In spite of the relatively weak bond, the molecules are aligned on the surface.[40] On the NiO(100) surface CO is oriented perpendicular to the plane of the surface such that the carbon atom is coordinated to Ni. In contrast, the axis of a NO molecule is tilted at 45° to the surface normal.[23] As with CO, the coordination is to Ni, though the bond takes place through the nitrogen atom.

A series of theoretical studies has been carried out on the bonding of CO to MgO and NiO.[23,45-50] The calculations all give binding energies that are far too small in relation to those obtained experimentally. However, agreement exists since the bond is based fundamentally on electrostatic effects: the ionic surface interacts with the multipole moments of the molecule. Covalent bonding components were not found in the given examples. In particular, it appears that the tried-and-tested Blyholder model[51] for transition metals cannot be used for the analysis of the bond between CO and a transition metal oxide surface. There are many reasons for this,[45-51] among which the most important is that the open d shell in NiO cannot hybridize with the energetically high-lying s orbital of $Ni^{2+}$ and thus loses the flexibility of the "preparation" of suitable bonding orbitals that is possible on the surface of a metal. The open d shell is thus strongly spatially localized such that in addition to the hindrance from the bulky oxygen atoms, a molecule cannot be bound through a σ-donor–π-acceptor interaction. Figure 4 provides a detailed comparison of the classical Blyholder bonding mechanism with that of the effective bonding mechanism of the examined oxide surfaces.

In the first case a metal band exists with considerable dispersion. In this metal band structure, the s- and d-metal atom orbitals are hybridized because their energies lie in approximately the same energy region. Unfilled metal bands interact with the filled 5σ orbital of the CO molecule and contribute to the formation of a σ-donor bond. Occupied bands can form a π-acceptor bond with the unoccupied 2π orbital of the CO molecule.

In the second case the metal atoms or ions are separated by the oxygen neighbors, such that the development of a band structure for the resultant strongly localized d states can be neglected to a first approximation. The typical ligand field splitting of a square pyramid with a triplet ground state is observed. Naturally, the oxygen orbitals develop a band structure whose energetic position is schematically shown (O 2p). Calculations show that the unoccupied s orbitals of the Ni ions are very strongly destabilized. Thus, only an exceptionally weak 5σ-d donor bond or none at all can be formed, particularly since the relevant $d_z$ orbital of the $Ni^{2+}$ is singly occupied. For a π-acceptor back bond, the CO molecule must move very close to the d orbitals; on a (100) surface this is prevented by the Pauli repulsion between the 5σ and 1π electrons and the electrons of the oxygen atoms. The situation with MgO is even more apparent, since $Mg^{2+}$ has formally no valence electrons.

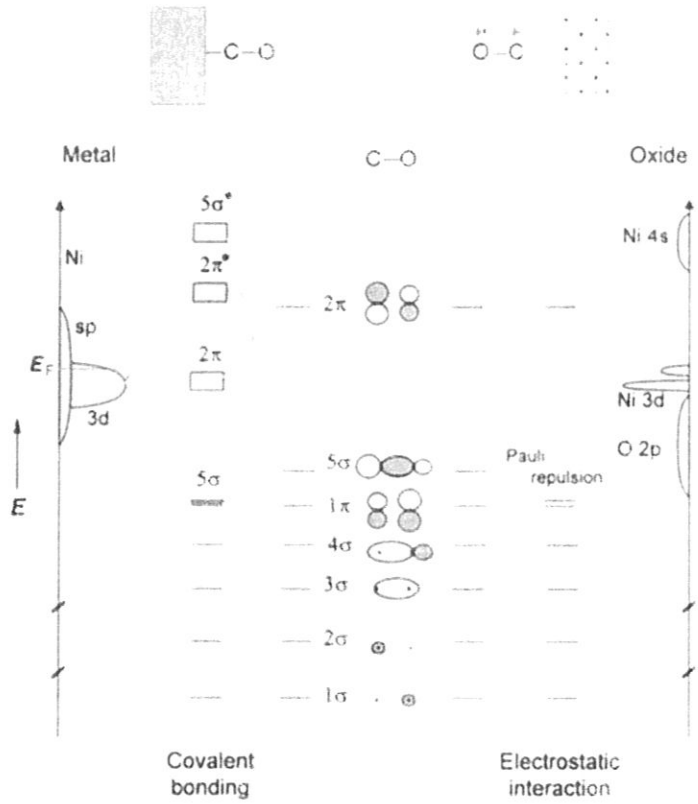


Figure 4. Schematic representation of the bonding of CO on transition metal surfaces (left) and oxide surfaces (right).

The changes in vibrational frequencies for CO and NO relative to those in the gas phase can also be understood in the context of an electronically dominated interaction. Here, three effects play a role. The first is the wall effect,[48] which takes into account that in a CO bond stretch, the carbon atom vibrates against a more-or-less rigid wall. This shifts the vibrational frequency to higher values. The second effect is dipole–dipole couplings: A chemical interaction which represents the third effect would lead to a lowering of the vibrational frequency provided that through this interaction the antibonding 2π orbital of the CO molecule is populated. A shift of this kind occurs for adsorbed NO.

For CO on MgO(100),[41-43] NiO(100),[44] and CoO(100),[47] the CO stretching frequencies are near or even slightly above that of the gas phase value. This is consistent with the above-mentioned electronic considerations. However, for NO there is a great deal of support that it not only electrostatically interacts with NiO(100) and CoO(100), since the NO stretching frequency is between 9 and 13 meV lower than that in the gas phase, which at the moment can only be explained succinctly through chemical interactions.[23,52]

Calculations by Staemmler et al. support this statement.[23] These calculations use the "cluster approximation" in which the molecule interacts with a relatively small part of the NiO surface that is described fully and correctly by ab initio methods. This cluster is then embedded in a half-infinite arrangement of point charges, in order to simulate the docking to the bulk crystal. Figure 5 shows an extremely simplified MO diagram. Two extreme cases—perpendicular and tilted NO—are compared.[23] In contrast to CO the 2π orbital is occupied, and lies energetical-

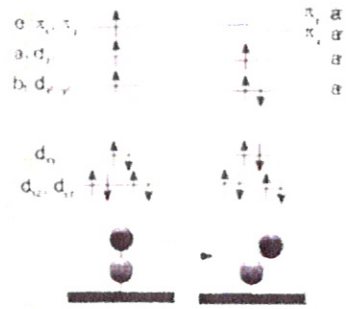

Figure 5. Schematic representation of the bonding of NO adsorbed on NiO(100) with perpendicular (left) and angled geometry ($C_s$ symmetry, right) from the single-electron picture.

ly at a clearly lower energy, thus nearer to the Ni d orbitals. Nevertheless, this orbital cannot interact in the perpendicular NO direction with the d orbitals for symmetry reasons. However, if the opposing symmetry is overcome by tilting the molecule, the $2\pi$ orbital can interact, forming a bonding and antibonding combination and with the corresponding occupation lead to a stabilization of the bond. Detailed calculations reveal that the configuration after NO adsorption shown in Figure 5 right is one of many possibilites. However, configuration calculations show that the angled configuration is the most stable. Evidently, one must be clear that the bonding on the oxide support layer, if it exists, can only be compared in the extreme case with the bonding in NO complexes. At any rate the calculated charge transfer between the systems on adsorption is very small.

### 3.3. Adsorption and Reactivity: Polar Surfaces

Polar surfaces are more reactive, even if their structure is well developed.[10, 11, 31, 53–57] Their preparation by epitaxy is just as possible as that of nonpolar surfaces. Reasons for the high reactivity are quite evident.[45–51] In general, the fundamentally higher surface potential is the source of the increased reactivity and strong molecule–substrate bond. In addition, local effects such as the changed coordination of the metal ions in the surface, which limits their ease of reachability for the molecules in the gas phase, and the large influence of local field strengths have to be taken into account. The local situation faced on a polar surface evidently also occurs in defects on nonpolar surfaces. For instance the oxygen site on a (100) surface: The microfacets in this case are (111) oriented. Needless to say the opposite situation is observed on the tip of a (100)-oriented crystal. Pacchioni and Bagus[45] have shown with help from SCF calculations the following trend: the interaction energy on such defects increases relative to that on (100) terraces even if the estimated absolute value is viewed with a certain amount of sceptisism due to difficulties that arise in the estimation of adsorption energies. Analogous conditions should be expected also for polar surfaces. However, in addition in this case there is the above-mentioned global surface potential, which can induce distinctive reconstructions of the surface. We would like to demonstrate this with two examples.

First let us consider the NiO(111) surface. It can be produced either as a relatively thick film ($\geq 50$ Å) on the Ni(111) surface by oxidation,[31] or as a relatively thin film ($\leq 10$ Å) on a Au(111) surface by oxidation of vapor-deposited Ni.[58] Films grown on Ni show a well-developed p(1 × 1) LEED diagram, regardless of their actual thickness. Analysis by vibrational spectroscopy, in this case electron energy loss spectroscopy (EELS), shows that OH groups are located on the surface.[31] This means that the surface has stabilized itself during the growth by uisng the impurities present in the gas, and thus created a situation like that shown in Figure 3d: the first layer is saturated with OH groups and in this way reduces its surface charge by a factor of 2, which is a necessity for stabilization. Removal of the OH layer by heating, leads to the intermediate formation in the ideal case of an OH-free NiO(111) surface, which is not electrostatically stable and thus reconstructs.[59] The above-mentioned octopolar reconstruction is observed (see Figure 3b). If water is added to the reconstructed surface with the p(2 × 2) LEED pattern, the final state leads again to a p(1 × 1) LEED pattern. We observed this event with a SPA-LEED apparatus[59] and with a focused $\mu$-LEED system.[60] A thin film on Au(111) shows that this is not a reversible phenonomen.[62] Furthermore, in this case the film forms in the reconstructed form and cannot be forced into the p(1 × 1) structure through the use of $H_2O$.

Figures 6 and 7 show the appropriate experimental data. LEED and structural data for the relatively thick NiO film on Ni are shown in Figure 6,[9] and the atomically resolved structure of the thin Ni film as an STM picture in Figure 7.[58]

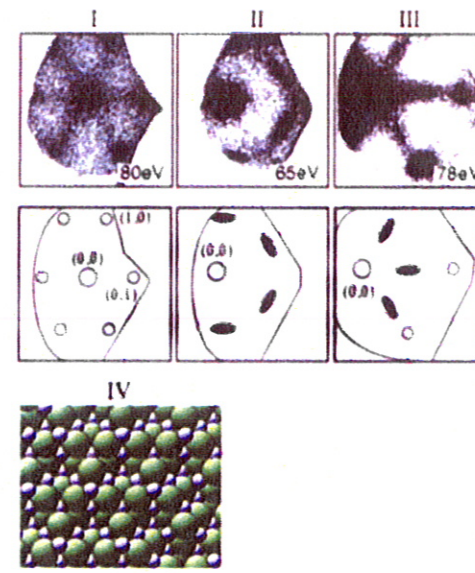


Figure 6. LEED pictures of the NiO(111)/Ni(111) system and their schematic representations (dark ellipses: superstructure reflections, light grey shaded circles: main structure reflections). I: Unreconstructed surface; II and III: p(2 × 2) reconstructed surface; IV: Model of the octopolar reconstructed NiO(111) surface.

It is assumed that the lacking influence from adsorbed $H_2O$ on the very thin film is attributed to the lack of a distinctive surface potential divergence, which could drive the process. This is observed during the reconstruction with the formation of (100) facets, which are arranged at an angle of 70° to the global (111) direction, and also confirmed by adsorption experiments.[52] If CO is adsorbed on an octopolar reconstructed surface, a global tilting angle of the CO axis is observed, which is consistent with that of the facets, if, as in the case of adsorption on NiO(100), a perpendicular ordering of the axis is assumed for CO.

This together with the surface reconstruction that accompanies the adsorption of $H_2O$ could have significance in real catalytic events, as Helmut Papp and co-workers have recently

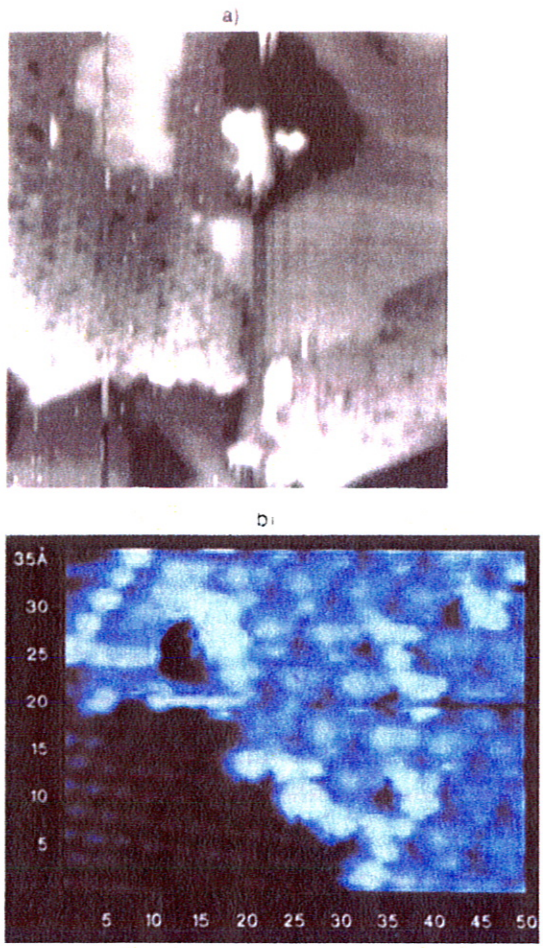


Figure 7. a) STM diagram of the p(2 × 2) reconstructed NiO surface, epitaxically grown on Au(111) (constant current topography (CCT), 250 Å × 250 Å, −5 V, 0.5 nA). b) Sample as in a) (CCT, 35 Å × 35 Å, −0.3 V, 0.5 nA).

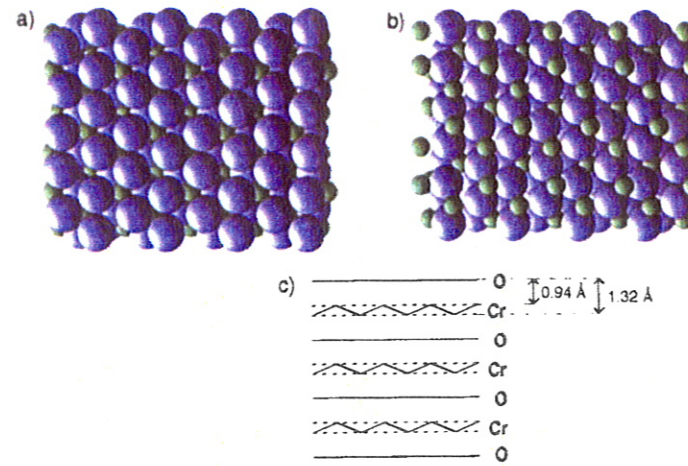


Figure 8. Different terminations of a $Cr_2O_3$ surface: a) by a complete layer of oxygen ions, b) by a complete layer of chromium ions. c) Schematic representation of the layer sequence.

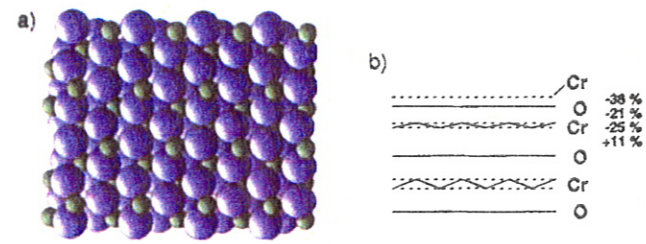


Figure 9. a) View of the reconstructed, depolarized $Cr_2O_3$(0001) surface. b) Schematic representation of the relaxation in the interlayer distance after surface reconstruction.

shown:[61] through topotactical decomposition of $Ni(OH)_2$, NiO powder can be produced whose crystallites show predominantly the (111) orientation. The activity of this powder was tested with the DeNOx reaction, that is the decomposition of NO with $NH_3$ to give $N_2$ and water. The activity was shown to only start at a temperature above 400 K. At this temperature the last thrust of water loss takes place, and the OH groups bound to the initially well-defined NiO(111) film begin to separate off as water. Thus the next logical step is to combine both processes, which leads to the conclusion that the water-free but reconstructed surface has sufficient energy to drive the DeNOx reaction, whereas this is not the case for the OH-covered surface.

As a second example we chose the $Cr_2O_3$(0001) surface, a polar surface of the corrundum type.[5] Schematic representations of the of possible structures of the terminated bulk are given in Figure 8.[62–64] These are unstable for the same reason as the corresponding structures with the rock salt structure. A reconstruction that resembles that shown in Figure 3a occurs on the $Cr_2O_3$(0001) surface. We know from ion-scattering spectroscopic measurements[65] and from LEED $I/V$ analysis[66, 67] that only half of the expected chromium ions lie on the surface after bulk termination. From the honeycomb structure only a hexagonal arrangement of Cr ions remains (Figure 9a), which, however, still gives the same LEED scattering pattern as the full layer. This pattern is, however, only observed at low temperatures (90 K).[64] On increasing the temperature a sharp scattering pattern of a $(\sqrt{3} \times \sqrt{3})R30°$ structure develops at 150 K, which at higher temperatures becomes diffuse.[64] The relaxation of the interlayer distances at 90 K is very pronounced and reaches deep into the solid.[67] This leads to the conclusion, as Figure 9b shows, that the surface chromium ions are nearly embedded in the oxygen layer. There are some indications for strong relaxations from theoretical approximations on $Al_2O_3$,[68, 69] which is isostructural to $Cr_2O_3$. The relaxations amount to 50% of the interlayer distances. Furthermore, the observed structural changes with increasing temperature point to dynamic processes. The temperature-dependent EEL spectra indicate that the ions could either undergo site changes or magnetic scattering in the antiferromagnetic material or small local surface distortions could occur;[64] however, very little is known about the exact mechanism.

Further indications of dynamic processes on films are obtained from adsorption experiments with oxygen.[57, 70, 71] If a clean $Cr_2O_3$(0001) surface is dosed with molecular oxygen, this will be adsorbed molecularly at 90 K. IR spectra (Figure 10) contain an absorption band at about 1000 $cm^{-1}$, which by exchange of $^{16}O_2$ for $^{18}O_2$ gives, in accord with the isotope effect, a small shift in frequencies.[71] The band is relatively wide, and experiments concerning the $O_2$ coverage, point to the presence of many different adsorbed $O_2$ species.[72] If the temperature is

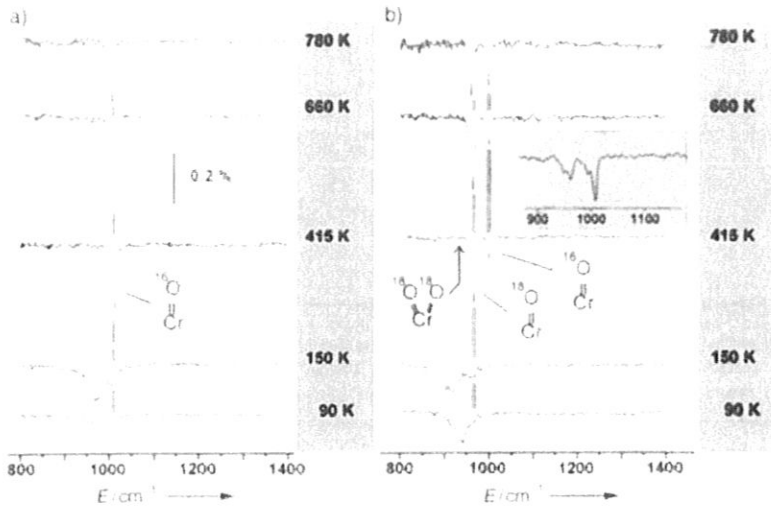


Figure 10. IR spectra of a $Cr_2{}^{16}O_3(0001)$ surface after dosing with 6L $^{16}O_2$ (a) and 6L $^{16}O_2$ (b), respectively, at 90 K, and subsequent heating to the given temperatures. The insert in (b) shows the spectrum of another preparation.

increased to 415 K, oxygen dissociates and chromyl groups are formed. The IR spectrum now contains a sharp, slightly asymmetric band. If the dissociation is monitored with isotope-labeled $^{18}O_2$, in addition to the $Cr\sim{}^{18}O$ band shifted by the isotope effect, the $Cr\sim{}^{16}O$ band is also present. Whereas the molecular $O_2$ adsorption occurs with no exchange with the oxygen in the lattice, $O_2$ dissociation and the formation of the chromyl groups leads to an exchange with lattice oxygen.

These observations allow a few conclusions to be drawn about the bonding state of the oxygen on the surface: firstly $O_2$ is known not to be IR active in the gas phase. Evidently, the adsorption leads to a noticeable change in the electronic structure of the molecule. Photoemission experiments[73] reveal that these changes possibly arise from a very small charge transfer from the surface to the molecule. Thus, this cannot be considered as a fully formed $O_2^-$ species even though the shift of the vibrational frequency from 1555 $cm^{-1}$[74] to 1010 $cm^{-1}$ would be consistent with this.

The observation of the $O_2$ vibration in the adsorbed state also allows conclusions to be made about the bonding geometry: If the molecule lays flat on the surface, the induced dipole can be screened from the electrons in the underlying layer, provided that the polarizability is sufficiently large.[75] This leads to an overlap of two opposing dipoles and thus to a disappearing transition dipole moment. In contrast, if in the other extreme case where the molecule is perpendicular to the surface, the overlap leads to a strengthening of the induced dipole moment. For the system considered here, we conclude that the adsorbed $O_2$ molecule does not lie flat on the $Cr_2O_3(0001)$ surface but end-on bound to a chromium ion. As already mentioned, after the $O_2$ dissociation a chromyl species develops. The IR absorption of the Cr–O double bond lies in the same frequency range as that of the modified $O_2$ bond. This is also evident from a comparison with the IR spectrum of $CrO_2Cl_2$.[76] The two relatively heavy Cl atoms represent to a good approximation the "surface" onto which the chromyl groups are bound. The vibrational stretches of the chromyl groups occur at 990 and 1000 $cm^{-1}$ for the symmetric and antisymmetric combination, respectively, of the two Cr=O vibrations.

We had initially expected that two chromyl bonds per chromium ion form on the surface, since the Cr=O band was always asymmetric and in many cases clearly split. This splitting could be attributed to the corresponding symmetric and antisymmetric combinations. However, there could also be two different chemical species with single Cr=O bonds on the surface next to each other. Isotope labeling experiments[70, 72] clearly indicate that only single Cr=O bonds form on the surface, and thus there must be two different species. If this is compared to the situations after dissociation from $^{16}O_2$ and from $^{18}O_2$ on a $Cr_2(^{16}O)_3(0001)$ surface, the expected band for the two $Cr={}^{18}O$ bonds is never found in one molecule. This result agrees remarkably well with the findings for polycrystallized $Cr_2O_3$.[77–79] Interestingly, chromyl groups form on the surface not only through adsorption of $O_2$ from the gas phase, but also by repeated heating of the clean surface. Isotope labeling experiments show that these groups form by oxygen diffusion through the film.[72]

The above-mentioned experiments indicate that the chromium ions on the surface are the active adsorption sites. This becomes even more apparent if, after coverage with oxygen, attempts are made to adsorb a further compound such as ethene or CO.[70, 73] Thermal desorption studies show that after saturated coverage with $O_2$ the adsorption of further particles is strongly reduced.

In contrast, if ethene or CO is supplied to a clean, that is not oxygen-covered, $Cr_2O_3(0001)$ surface, a bond is formed to the support.[70, 73] Figure 11 shows the results from an IR spectro-

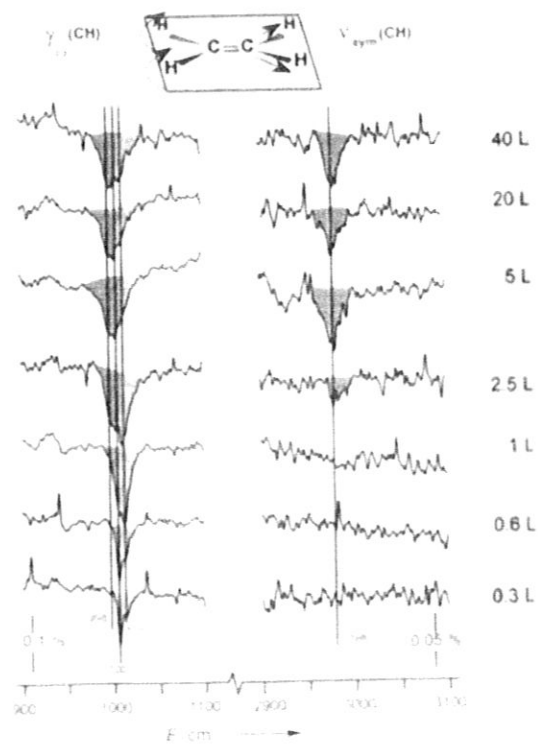


Figure 11. IR spectra of a $Cr_2{}^{16}O_3(0001)$ surface after dosing with different amounts of $C_2H_4$ at a surface temperature of 90 K.

scopic study of the coverage with $C_2H_4$ at 90 K. The frequency regions of the CH bending vibration $\gamma_{as}$(CH) and the symmetric CH stretching vibration $\nu_{sym}$(CH) are shown. Even for small coverages the bending vibration begins to shift in frequency with a dose of 1 L. A measureable vibrational signal occurs from about this amount of coverage. As for the case of the oxygen adsorption discussed, the absence of the stretching vibrational signal points to an ethene molecule oriented parallel to the surface, possibly bound to a chromium ion. The photoemission measurements provide evidence of a small charge transfer from the molecule to the surface. At a large dosage the population takes on a physisorbed state, which shows, through the occurrence of both IR bands, that there appears to be no detectable, preferred orientation relative to the surface.

When these experiments are carried out under ultrahigh vacuum conditions, chemi- and physisorption are fully reversible, which means that with a temperature increase the ethene desorbs completely. In contrast, if the adsorption is performed at about 1 bar and about 400 K, a reaction on the surface takes place that we have interpreted as a polymerization of ethene,[73] which is in complete agreement with data from the Zecchina group.[80] After the polymerization, adsorbed OH groups are formed. Such a finding is not completely surprising, since chromium oxide is part of the well-known Phillips catalyst for the synthesis of polyethylene.[81, 82] In addition, similar experiments have already been carried out on polycrystalline samples.[80] Based on the results described here, more can now be said about a possible mechanism for this technically important reaction: $C_2H_4$ is adsorbed side-on on to a $Cr^{3+}$ ion through a small charge transfer, resulting in changes in the electronic states of the $Cr^{3+}$ ion, as we could show by EEL spectroscopic analysis of the surface excitations of the chromium ions.[73]

Hitherto, there were no experimental results on thin film systems that indicated the direct formation of $Cr^{2+}$ on the surface as a consequence of ethene adsorption. Rather, the more accurate picture is one in which an interaction between ethene and a coordinatively unsaturated chromium ion is the active center for ethene polymerization.[80–82] This result corresponds to the classical bonding theory of a π-bonded ethene molecule.

In contrast, CO bonds in a nonclassical way on a $Cr_2O_3$(0001) support layer. Angle-resolved photoelectron spectra[66] support a case in which the CO molecule lies flat on the surface, and the lone pairs of electrons on carbon (5σ) and on oxygen (4σ) are involved in the bond. This is further supported by the shifting of the ionization energies of the appropriate states.[66, 83] The behavior of CO/NiO(100),[48] in which the interaction exists only through the carbon atom, deviates considerably from that of CO/$Cr_2O_3$(0001).[83] In contrast, it seems that NO on $Cr_2O_3$(0001) is bound in a tilted manner in a similar way as on NiO(100).[23] How can the CO/$Cr_2O_3$(0001) interaction be modeled? We know now that in contrast to previous assumptions the $Cr_2O_3$ surface is very strongly relaxed. This means that the chromium ions are not as exposed on the surface as was previously thought.[84] It is, thus, not likely that the CO molecule can simultaneously form bridging interactions with two chromium ions. On the contrary, it is more likely that CO, similar to ethene, is bound through a single Cr ion (Figure 12). Thereby, a π bond is formed, which leads to a shift of the 1π ionization energy to a higher value. Only one component of the 1π orbital is influenced by this shift because of the high symmetry of the adsorbate site. However, since CO adopts a position at an angle to the surface plane, hybridization effects must be taken into consideration, so that a clear separation into two components is not possible. The 5σ and 4σ orbitals of CO in this arrangement contribute very little to a chemically bonding interaction, but experience the pronounced Pauli repulsion of the closed-shell oxygen ions, and are therefore shifted to higher binding energies. This shift resembles the pure electrostatic shift of the 5σ orbital in the CO/NiO(100) system (see Figure 4).[44] As a result of the changed adsorption geometry, in this case both σ orbitals are influenced.

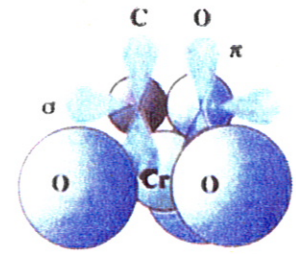

Figure 12. Schematic representation of the interaction of CO (with its $p_z$ and $p_x$ orbitals) with a Cr ion on the reconstructed $Cr_2O_3$(0001) surface.

The bonding of CO on the support layer comprises two opposing contributions: the stabilization by the π orbital and the destabilization by the repulsive σ interactions with the substrate (see Figure 12). The attempt to derive a charge transfer between the CO molecule and the surface in the photoelectron spectrum was not successful.[84] CO produces the only adsorbate system up to now on $Cr_2O_3$(0001) for which an ordered structure has been found. The LEED picture has $(\sqrt{3}\times\sqrt{3})R30°$ symmetry and could be confused with the pattern of the phase transition of the substrate. However, the *I/V* behavior differs clearly for the superstructure reflections of the two structures.[85] Furthermore, the CO superstructure is also detected at low temperatures at which the phase transition is not active. Whether the interaction of the CO molecules with the Cr ions on the surface stabilizes or influences the phase transition is still not clear. The adsorption of a number of other different compounds leads, however, to the disappearance of the phase transition.

## 4. Experiments on Metal-Deposited Modified Oxide Surfaces

The binary systems discussed in Section 3.3 can be modifed by the introduction of additional chemical components. We concentrate here on the modifications achieved by deposition and growth of ultrathin metal films. The systems created in this way[87–117] can be considered as model systems for disperse metal catalysts. Thus, their study has a certain practical relevance.

Typical metal support systems are those in which the metal is a transition metal, and the support is, for example, composed of $SiO_2$, $Al_2O_3$, or MgO. The methods discussed in Section 3.3 can be employed to produce well-ordered layers of MgO[41–43, 118–120] and $Al_2O_3$.[121–129] The preparation of ordered $SiO_2$ layers still gives difficulties.[130] We have focused our attention until now on the support system $Al_2O_3$, and thus in the following, initially the structure and properties of the support,[121, 126] as well as the possibilities of its chemical modification by functionalization[131] will be considered, and thereafter the growth, morphology, adsorption, and reaction behavior of the metal films deposited.[131–142]

### 4.1. Structure of a Support

A well-ordered, thin $Al_2O_3$ film can be generated on a (110) surface of a NiAl alloy single-crystal by oxidation and tempering at 900 K.[121, 126] The choice of this system has several advantages. If one tried to produce an $Al_2O_3$ film on an Al substrate, a film would be produced that covers the whole surface, and thus to order this film, the temperature would need to be raised to such an extent that the substrate would melt. In contrast, NiAl has a high melting point of 1638 °C. $Al_2O_3$ is produced on the surface by oxidation; the freed Ni dissolves in the NiAl bulk through heating because the thermodynamically most stable phase in the NiAl system is the nickel-rich $Ni_3Al$. The dissolution of nickel in the bulk can be monitored, for example, by ESR spectroscopy.[143] The thickness of the film was determined to be 4–5 Å from angle-dependent X-ray photoelectron spectroscopy[144] and from Auger spectroscopy.[145] The stoichiometry of the film corresponds within the limits of experimental error to that of $Al_2O_3$.[121] Photoelectron spectroscopy and EEL spectroscopy were used to show that the film contained no metallic Ni and no NiO.[121] The film is chemically unreactive, and CO adsorbs on it only at low temperatures (<80 K),[123, 124] whereas CO binds to the NiAl substrate up to significantly higher temperatures.[146] Thermal desorption studies confirm the film formed covers the whole surface of the alloy. Figure 13 shows a scanning tunneling microscope (STM) image[132] of the growing $Al_2O_3$ film. The STM image shows two terraces of the NiAl substrate, and above this an extended domain of the $Al_2O_3$ film, characterized by the striped pattern in the direction of the twist of the domain. The $Al_2O_3$ film is remarkable in the way it spreads itself over the steps of the substrate like a "carpet", a phenomenon that is known, for example, for the growth of alkali metal halide films on elemental semiconductors.[147]

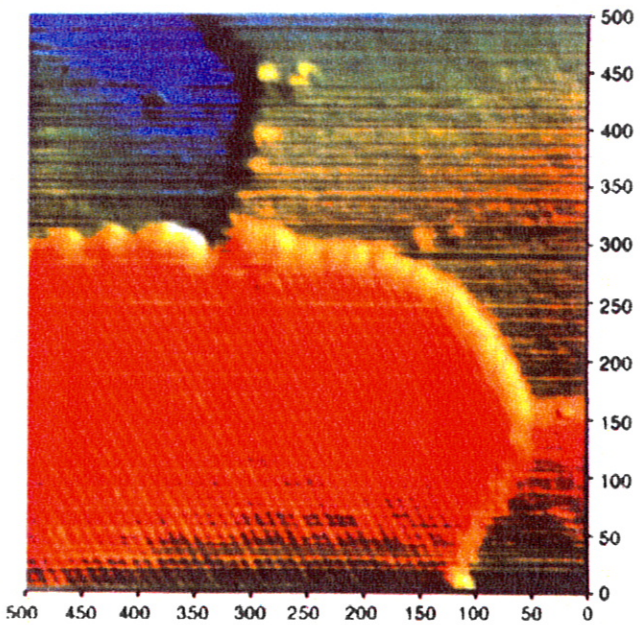


Figure 13. STM diagram (CCT, 500 Å × 500 Å, +4 V, 2 nA) of a partly oxidized NiAl(110) surface. The $Al_2O_3$ film can be identified by the characteristic striped pattern (bottom left). A step of the NiAl substrate can be seen above [132].

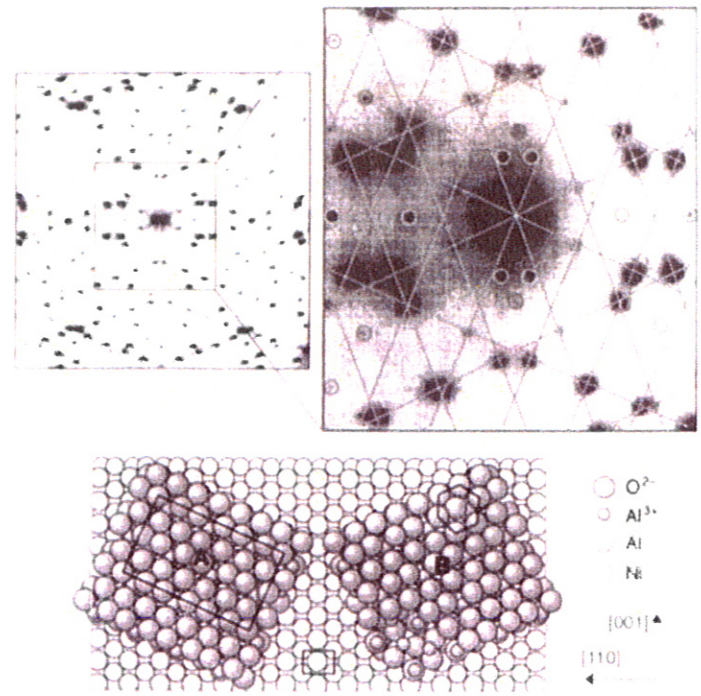


Figure 14. Top: Global LEED picture (85 eV) of the $Al_2O_3$/NiAl(110) system as well as the enlarged representation of a region around the (0,0) reflection. The reflections that appear in addition to those of the oxide (marked grid) are attributed to double scattering on the substrate and oxide structure (incommensurably grown along [001]). Bottom: Schematic structural model derived from $\gamma$-$Al_2O_3$. The size of the unit cell of the oxide superstructure determined from the diffraction pattern is marked.

Figure 14 shows the electron scattering pattern of the film together with a schematic structural model.[121] The LEED picture, as indicated, still shows the reflections of the substrate. Superimposed onto the substrate spots are the reflections derived from a superposition of two domain LEED patterns, as indicated in the diagram. The double diffraction reflections through scattering on the $Al_2O_3$ film and substrate exist but are of a weak intensity (see Figure 14).[122] The two domain directions A and B are at an angle of 24° to each other. This twist is forced by the arrangement of the large, nearly square unit cells on the (110) NiAl surface. The arrangement of the $Al_2O_3$ layer in the (110) direction is substrate-related and commensurable, in the perpendicular direction, however, incommensurable.

Figure 15 shows an STM image of the domain interface,[126] which has no atomic resolution, rather the protrusions show a global variation of the electronic structure about the marked

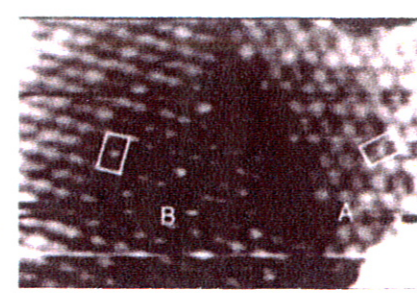


Figure 15. STM image of the $Al_2O_3$/NiAl(110) system (CCT, 210 Å × 130 Å, −2 V, 0.5 nA). The unit cells of the differently oriented domains A and B are marked (cf. Figure 14).

unit cells. The STM image was recorded under conditions at which electrons from the oxide layer tunnel to the tip of the scanning tunneling microscope. Since the occupied density of states of the oxide begins at about 4 eV below the Fermi energy of the alloy substrate, high tunneling voltages are required. Therefore, the distance between the tip and the substrate is relatively large, and the lateral resolution is limited. If small tunneling voltages are used, the electrons tunnel mainly from the substrate through the film to the tip. This can be used to reproduce the atomic structure of the NiAl layer immediately beneath the $Al_2O_3$ film.

Figure 16a shows an image of the hidden layer in the NiAl substrate, directly bordering the oxide with atomic resolution, which was recorded under the above tunneling conditions.[126]

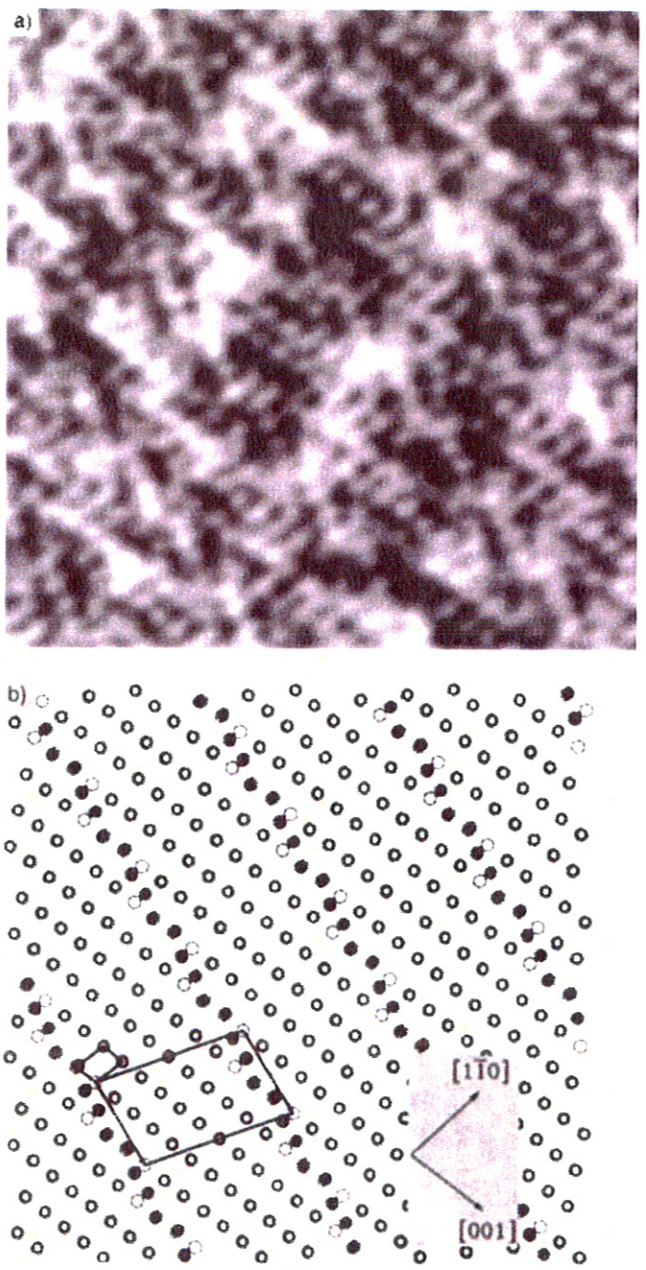


Figure 16. a) STM image of the $Al_2O_3$/NiAl(110) system (CCT, 90 Å × 90 Å, −1 V, 1.5 nA); b) schematic representation of the atomic structure of the NiAl(110) layer beneath the oxide layer (derived from (a)).

Together with the schematic representation in Figure 16b it is clear that through a regular displacement of every fourth atom the incommensurability of the $Al_2O_3$ unit cell is compensated in this direction. The existence of this interface also clarifes why the double scattering reflections in the LEED image were so weakly pronounced.

The thickness of the $Al_2O_3$ film is comparable with two Al–O double layers, as shown schematically in Figure 17. The $Al_2O_3$ film is oxygen-terminated, as we know from ion-scattering spectroscopic experiments.[133–135] Both the intensity distribution in the electron scattering pattern and the measurements of the $Al_2O_3$ band structure by angle-resolved photoelectron spectroscopy hint at the formation of hexagonal oxygen layers.[121]

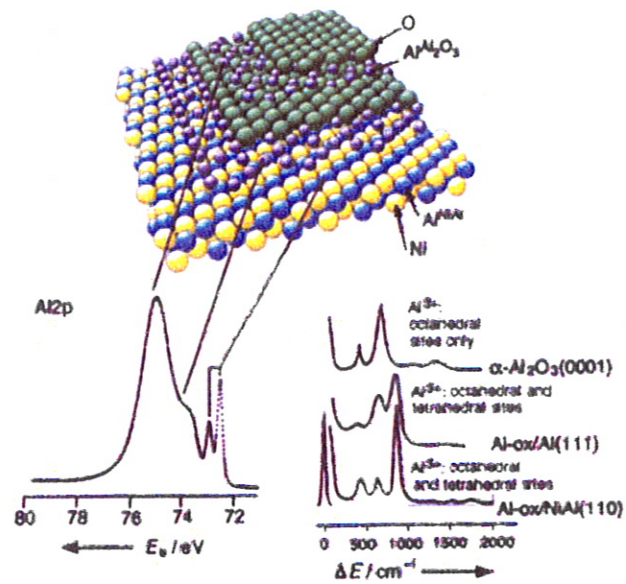


Figure 17. Top: Schematic buildup of the $Al_2O_3$/NiAl(100) system. Bottom: High-resolution photoelectron spectrum (left, $h\nu = 150$ eV, perpendicular emission) and HREEL spectrum (right). Substrate, interface, and oxide components are clearly separated in the photoelectron spectrum ($E_b$ = binding energy). The HREEL spectrum of the $Al_2O_3$ film on NiAl(110) is compared to those of Al(ox)/Al and α-$Al_2O_3$ ($\Delta E$ = energy loss).

Additional evidence for the formation of the layer is obtained from photoelectron spectra in the region of the Al-2p core electrons.[121] The photoelectron spectroscopic signals of individual layers in the film are assigned in Figure 17: The sharp doublet arises without doubt from the alloy support layer; the weak shoulder at about 74 eV must stem from the interlayer region, since it returns strongly in terms of its relative intensity when the spectrum is recorded at grazing electron emission, that is, lower escape depths of the electrons;[144] the most intensive signal in the photoelectron spectrum stems from the fully oxygen-coordinated Al ions. The nature of the coordination environment (octahedral or tetrahedral) of the Al ions is hard to decipher from this information alone. Similar information is provided in Figure 17 (bottom right) from the phonon spectrum of the film,[121] which was recorded by using electron loss spectroscopy. Comparison with the spectra of α- and γ-$Al_2O_3$ leads to the conclusion that the coordination corresponds more to that of γ-$Al_2O_3$ than that of α-$Al_2O_3$. This means that tetrahedrally and octahedrally surrounded Al ions are present.

We have thus achieved an extensive characterization of the film and established that we are dealing with a well-ordered $Al_2O_3$ film, which is free of hydroxy groups and which fully covers the surface. Evidently, this film cannot correspond in every way to a bulk single crystal, since in the direction perpendicular to the surface the thickness of a unit cell of $\gamma$- or $\alpha$-$Al_2O_3$ is not achieved. Nevertheless, it appears that in many ways the properties of this film are those typical for $\gamma$-$Al_2O_3$, and the layer thickness has only a limited influence on the observed properties.

The film prepared in this way can now be directly covered with metal, but it can also be chemically modified prior to the introduction of the metal.[131] Thus, it has been possible to study the influence of functional groups on the $Al_2O_3$ surface on the growth and reactivity of thin metal films: Of special significance in this context are hydroxy groups on the $Al_2O_3$ surfaces, and in the following the ways in which chemically modified films can be prepared will be discussed briefly.[131, 148–153]

The basic concept is the following: Metallic aluminum is absorbed on to the ordered $Al_2O_3$ film and then the layer thickness can be increased by oxidation with either pure oxygen, or by oxidation with $H_2O$ a somewhat thicker hydroxylated aluminum oxide layer is achieved. This process can be monitored by photoelectron spectroscopy (Figure 18).[154] The bottom

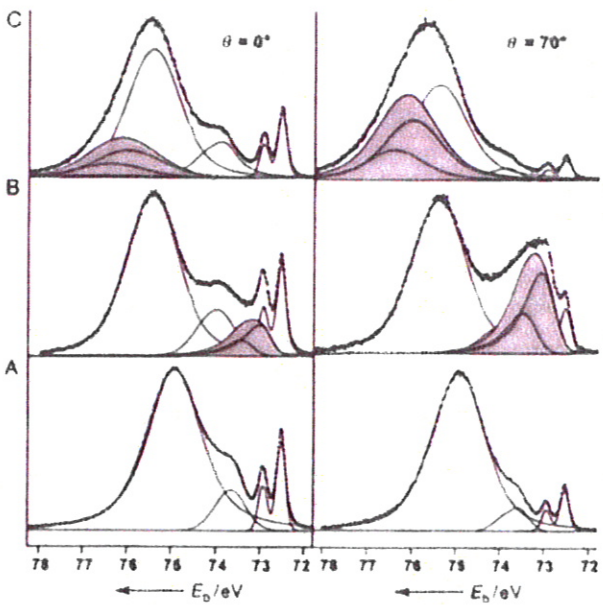


Figure 18. Al 2p photoemission spectra of the chemically modified $Al_2O_3$/NiAl(110) surface ($h\nu = 150$ eV grazing (70°) and perpendicular emission (0°)). A: Clean $Al_2O_3$ film; B: After deposition of 1 Å Al at 300 K; C: After $H_2O$ exposition at 90 K and subsequent warming to 300 K.

spectra (A) are those of the clean $Al_2O_3$ film, on the left hand side by perpendicular electron emission, and on the right hand side by grazing electron emission. Deposition of a part of a monolayer of metallic aluminum leads to the spectra B. From the production and the comparison with different spectra recorded at different angles of emission, it can be seen straight away that Al lies on the surface of the $Al_2O_3$ layer. Notably, in addition to the appearance of new bands, the whole spectrum is shifted to a smaller energy range. This is attributed to the fact that depending on the charge polarization in the interfacial layers, potential differences occur through the insulator layer. These differences can also be discussed in terms of band bending,[131] and lead to these shifts. Hydroxylation with water leads to a conversion of the metallic aluminum to the ionic form and to the top spectrum in the series (C). At the same time, the O 1s spectrum indicates the formation of a shoulder, which is typical for the presence of hydroxy groups. It is not surprising that through this process the order of the surface is changed, though it is by no means fully lost. The concentration of functional groups can be controlled by varying the dosage of aluminum. Evidently, it is conceivable that the formed OH groups can be used to further functionalize the surface.

### 4.2. Morphology of Metal Deposits

Metals can be deposited on clean and on chemically modified surfaces. Figure 19 shows two STM images of metal deposits on a clean $Al_2O_3$ surface—after deposition of 1/3 of a monolayer of silver,[132] and after about the same amount of Pt was deposited on the same substrate.[135] The substrate was at room temperature. Owing to the relatively high mobility of Ag, large particles form that deposit on the pronounced step defects of the surface (Figure 19b). In contrast, the mobility of Pt is reduced to such an extent that the platinum particles nucleate on the terraces. The competition between the interaction between metal and oxide and the thermal energy clearly decides on these processes. The adsorption energy $E_{ads}$ is described by the classical Young

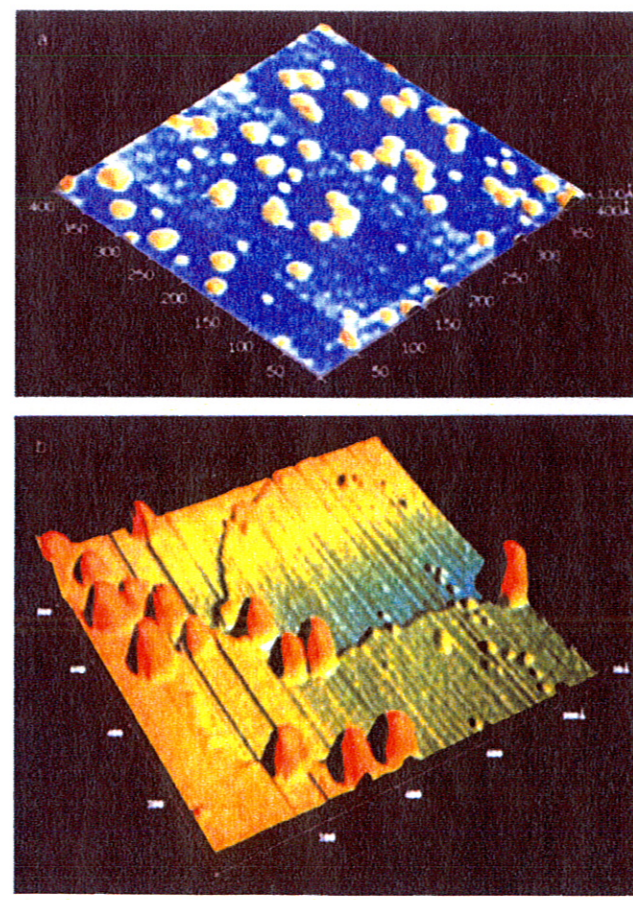


Figure 19. STM images of the $Al_2O_3$/NiAl(110) system after metal deposition: a) Pt growth at 300 K (CCT, 400 Å × 400 Å, −4 V, 0.8 nA), b) Ag growth at 300 K (CCT, 900 Å × 900 Å, −0.6 V, 0.5 nA)

approximation [Eq. (b)],[155–157] for which approximate values are known for the first two interaction energies, but the oxide/metal term is usually not known.

$$E_{ads} = E_{oxide/gas} + E_{metal,gas} - E_{oxide/metal} \quad (b)$$

Whether the metal particles move at a given temperature depends on $E_{ads}$. If $E_{ads} < 0$, full coverage is attained, that means a layer growth of the Frank–van der Merwe type. If $E_{ads} > 0$, three-dimensional islands are formed (Volmer–Weber growth mode).[157] If a layer-by-layer growth is replaced at a known layer thickness by a three-dimensional growth, it is referred to as a Stranski–Krastanov mode. Naturally, the detailed defect structure of the substrate and the introduced particles play an important role for these processes, since the defects of the oxide layer are nucleation centers for the deposited particles, as is apparent from Figure 19.

However, it's not just a case of the existence of defects per se but also their nature. Palladium, for example, has a growth behavior that is influenced by the existence of domain interfaces, as well as by the steps in the substrate and point defects in the oxide layer.[137] This is illustrated in Figure 20a, in which Pd was deposited at 90 K. The Pd particles partly decorate the domain interfaces, as can be seen in the figures. In addition, there are particles on the terraces. If the same amount of Pd is separated off at room temperature, the mobility is increased and clearly larger aggregates form. Some of the aggregates in Figure 20b adopt the form of small crystals. That these crystals are limited by planes with a (111) orientation is apparent from the electron scattering diagrams, such as that shown in Figure 20c.[137] The oxide reflections are two diffuse, but clearly definable, hexagonal (111) superstructure reflections rotated 12° towards each other. The double reflections stem from the growth of the particles on both the $Al_2O_3$ domains.

Figure 21 shows by using the (0,0) reflection as an example, the shoulders of the reflection, which, after deposition of Pd at two temperatures, become clearly defined at logarithmic intensity. From the form and the energy dependency of the shoulder in the LEED reflection profiles, that is the dependency on the energy of the scattered electrons, a well-documented analysis[158, 159] provides information about the average island size, island distance, island density, and number of atoms per island (see Figure 22). At 300 K the size of the islands reaches a plateau (Figure 22A, I). At this point an equilibrium between nucleation, diffusion, and growth is reached. Only if there is more than 12–15 Å of material deposited does the average island size grow further, through coalescence processes, that is the fusing together of the islands. The islands then have a regular form with well-developed facets that are crystallographically well-oriented. This is also borne out in the energy dependency (Figure 21 left). Clear in-phase and out-of-phase relationships between

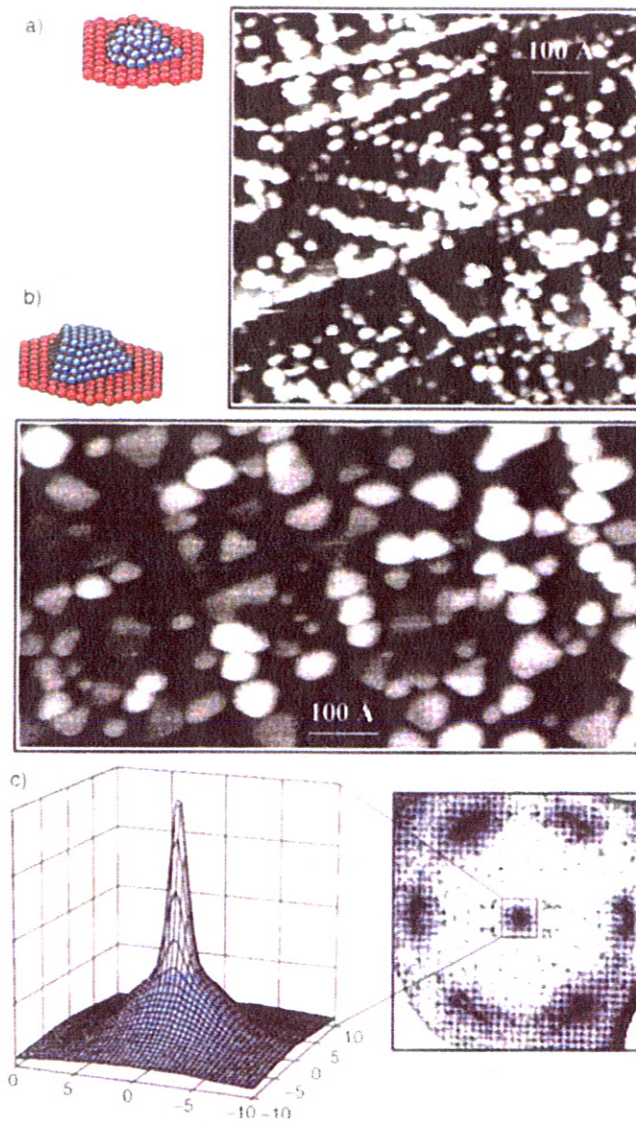


Figure 20. Pd growth on $Al_2O_3$/NiAl(110): a) STM image for growth at 90 K (CCT, 1.6 V, 2.2 nA). b) STM image for growth at 300 K (CCT, +0.4 V, 0.5 nA). c) LEED image after deposition of 20 Å Pd at 300 K (right, overview, 85 eV) as well as the intensity profile of a region around the (0,0) reflection (left $k_{\perp}$ in $\%G_{1\bar{1}0}$ is plotted on the axes; $k_{\parallel}$ is the wave vector with respect to the distance of the NiAl(110) reflections in the [1$\bar{1}$0] direction; 50 eV).

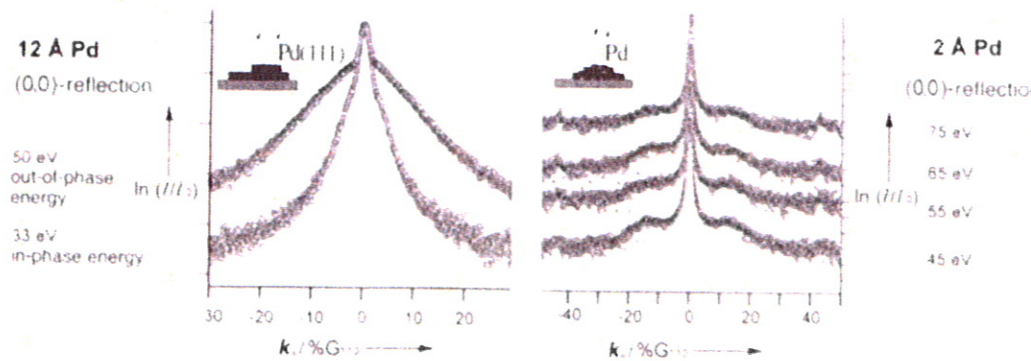


Figure 21. Intensity profile of the LEED (0,0) reflection after Pd deposition on $Al_2O_3$/NiAl(110) at different temperatures and electron energies. Left: Growth at 300 K, right: Growth at 90 K.

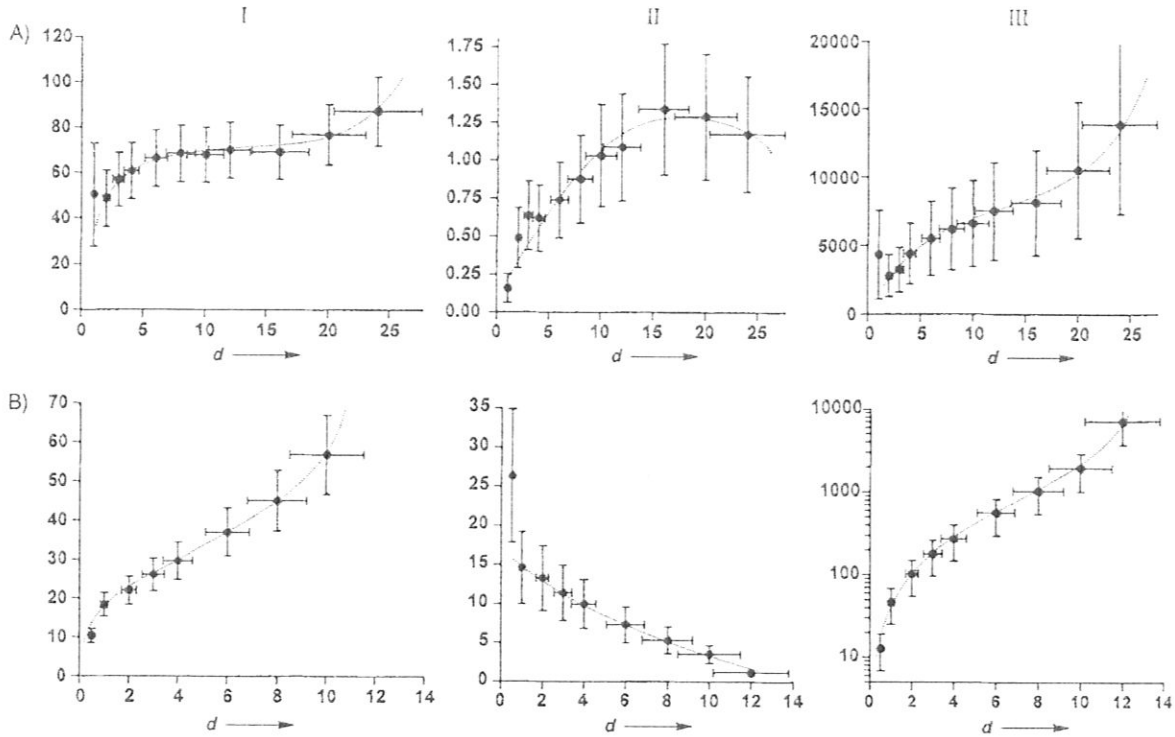


Figure 22. Variations in several of the quantities characteristic for the growth behavior for the deposition of Pd on $Al_2O_3$/NiAl(110), derived from LEED reflection profile analysis. A) Growth at 300 K, B) growth at 90 K; I: Average island size in Å, II: Island density in $10^{12}$ cm$^{-2}$, III: Average number of atoms per island; *d* nominal film thickness in Å.

the rays scattered on different terraces of the growing metal particles are again apparent in the reflection profiles. This is not the case for deposition at 90 K (Figure 21 right). A pronounced shoulder is still observed for the (0,0) reflection, but an energy dependency such as that at 300 K is not observed. Also the island growth shows clear differences relative to that seen at 300 K. Particularly characteristic is that no drop to a plateau is observed (Figure 22 B, I). This is possibly linked to the impaired diffusion during the deposition at 90 K. Nucleation centers are among others the domain interfaces on the $Al_2O_3$ layer, but pronounced nucleation also occurs on the terraces.

Figure 22 II and III provide a comparison of the derived island densities from the results discussed above and the number of atoms per island, respectively. As mentioned above indications are that at 300 K in the range up to a layer thickness of 10 Å the density of island sites increases strongly (II). Evidently, a considerable number of the islands is not produced at the start of the growth process by heterogeneous nucleation at strongly favored centers, but instead only in the latter stages either by homogeneous nucleation or nucleation at weakly favored adsorption sites. Also the number of atoms per island (III) shows the discussed growth phases; notably, even at low metal coverages large aggregates of more than a 1000 atoms can be formed. At 90 K the situation is clearly different. The rapid increase of island size originates from the fact that the very high island density of $10^{13}$ cm$^{-2}$ is achieved even by small coverages. Coalescence processes that begin early on allow the island density to steadily fall. This growth behavior has as a consequence that the number of atoms per island varies as a function of the amount of metal deposited over a large region. Under these conditions both the smallest particles with the least number of atoms as well as the very large aggregates are accessible.

For Pd many different metal deposits could be studied in this detailed manner. Rhodium shows a growth behavior similar to that of Pd.[131] A special feature for Rh is the strong nucleation tendency along one certain defect structure, particularly that of the antiphase domains of the oxide film.[131] We will not consider this aspect in any more detail here.

Figure 23 summarizes the growth behavior of the different metals on the $Al_2O_3$ film studied up to now and comparisons are made by using examples of the reflection profiles at 90 and 300 K. A characteristic of the growth of Ag at 300 K is the formation of larger aggregates, which leads to an extremely small outer shoulder that is hardly separable from the central

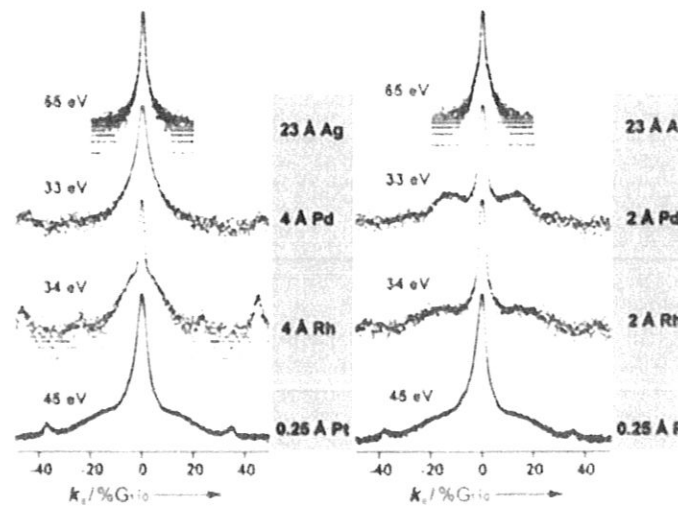


Figure 23. Comparison of the characteristic intensity profiles of the (0,0) reflection for Ag, Pd, Rh, and Pt growth on $Al_2O_3$/NiAl(110) at growth temperatures of 90 (right) and 300 K (left). The intensity is plotted logarithmically.

reflection. The large diffusion length of Ag leads to larger aggregates even at 90 K. This behavior corresponds to that of Ag on massive $Al_2O_3$ single-crystal surfaces.[150] The opposite extreme case with a well-pronounced shoulder is represented by the $Pt/Al_2O_3$ system. At both 90 and 300 K, small two-dimensional islands form due to the strong interaction. These offer possibilities to study substrate-induced changes of the properties of metal films.[9, 132, 133] Pd and Rh are categorized somewhere between the two extreme cases; Rh interacts somewhat stronger with the substrate than Pd. Thus, in terms of the strength of their interaction derived from the growth behavior with the oxide, the metals are arranged as follows: Pt > Rh ≥ Pd > Ag. This sequence is consistent with the formation enthalpies of the corresponding oxides.[161] ($\Delta H_f^{\ominus}$(AgO): $-12.1\ kJ\,mol^{-1}$, $\Delta H_f^{\ominus}$(PdO): $-85.4\ kJ\,mol^{-1}$, $\Delta H_f^{\ominus}$(RhO): $-90.1\ kJ\,mol^{-1}$, $\Delta H^{\ominus}{}_f(PtO_2)$: $-172.0\ kJ\,mol^{-1}$. This comparison, however, can only be interpreted as a hint towards considerations of the stability.

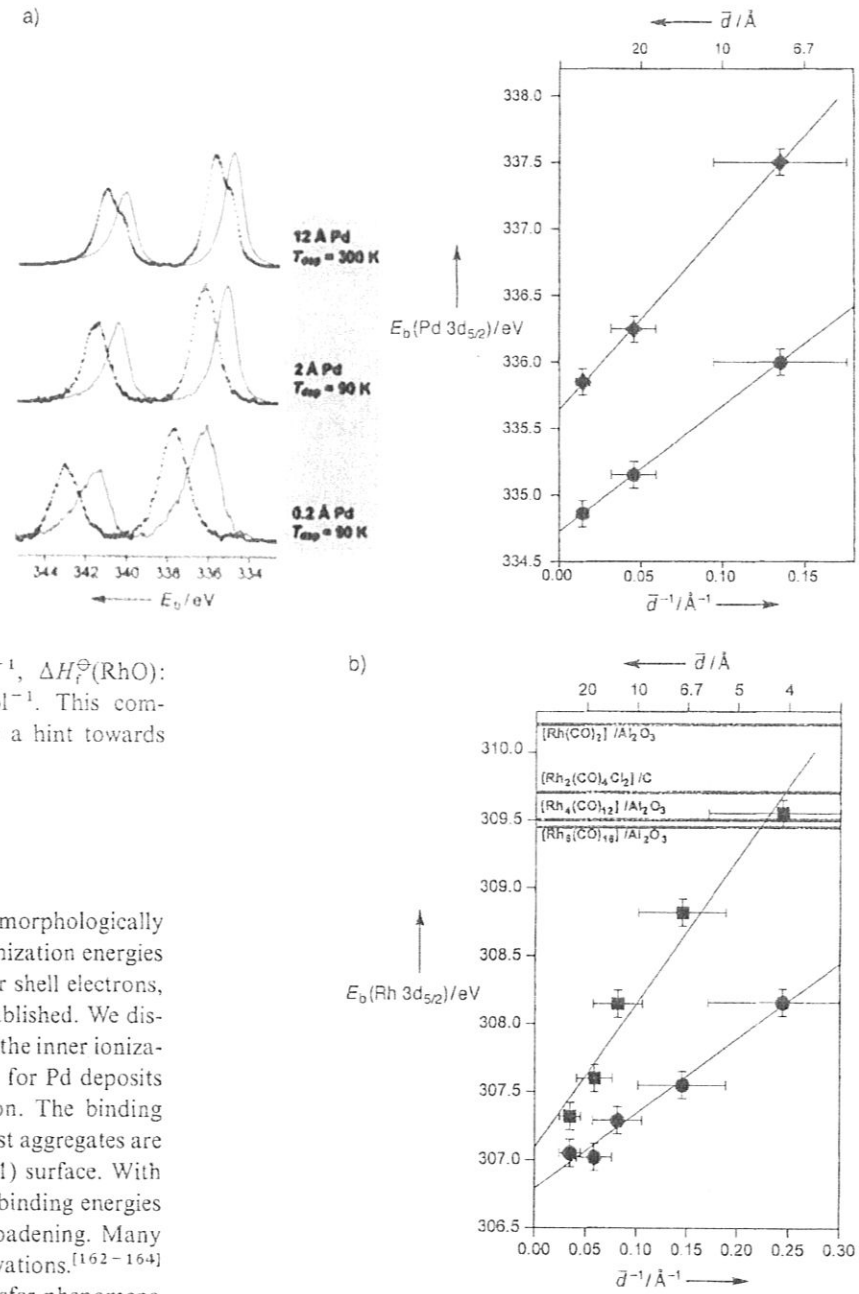


Figure 24. a) Left: Pd 3d photoelectron spectra ($h\nu$ = 420 eV) for different Pd deposits on $Al_2O_3$/NiAl(110), in each case before (solid line) and after saturation with CO at 90 K (dotted line; 20 L CO). Right: Plot of the binding energy of the Pd surface components as a function of the average particle size $\bar{d}$ for the CO-free (•) and the CO-saturated systems (•). b) Plot of the binding energy of the surface components as a function of the particle size for CO-free (•) and CO-saturated Rh deposits (▪). For comparison, the results for carbonyl compound deposits are given [179]. The best fits in (a), right, and in (b) are based on the Coulomb energy of the final state.

### 4.3. Electronic Structure and Adsorption

Photoelectron spectra can be recorded of the morphologically characterized systems.[138–140] Both for the ionization energies of valence electrons and also for those of inner shell electrons, the dependency on the particle size can be established. We discuss for the clean, adsorbate-free particles only the inner ionizations. Figure 24a summarizes some 3d spectra for Pd deposits that were recorded with synchrotron radiation. The binding energy and the line width observed for the largest aggregates are practically the same as that of the solid Pd(111) surface. With decreasing particle size, a clear shift to higher binding energies is observed together with a significant line broadening. Many effects could contribute to both of these observations.[162–164] Generally, it can be said that both charge transfer phenomena such as initial-state effects and also influences, which only arise in the ionized state of the system, could play a role. The discussion of line widths is especially difficult.[162, 163, 165–168] One can at the moment only speculate that the nonequivalence of the different metal atoms within the differently sized aggregates and the interaction of some of the metal atoms with the substrate combined with the final state effects are responsible for the spread.

In contrast, the interpretation of binding energy shifts, which are graphically summarized on the right of Figure 24a for Pd aggregates and in Figure 24b for Rh aggregates, is somewhat clearer:[164, 169] Specific metal–support interactions,[166] in the sense that charge is transferred from the metal to the support, can be discussed by using initial state effects. The discussion of final state effects is here also urgently necessary, since the screening of the positive charge formed by ionization leads to clear binding energy shifts. Whilst for a bulk crystal a fully delocalized positive charge results, the charge delocalization is limited for a metal aggregate not centrally bound to the substrate. Therefore, a charge distribution builds up on the particle, whose size depends on the average radius of the particle according to Equation (c),[164, 169] and the binding energy shifts to

$$E_c \propto R^{-1} \qquad (c)$$

higher binding energies as the radii become smaller. There are numerous experimental results[162–169] that are in accord with Equation (c) and with the explanation of the binding energy

shift described in Figure 24b. The shifts are generally attributed to final state effects. With a pronounced influence of charge transfer in a nonionized system, one would expect a strong influence on the bonding energy of the substrate, which, however, in our case is only 10% of the total effect. Possible reasons why pronounced charge transfer effects were observed with Pd[170-172] and Ni deposits on $Al_2O_3$ layers, which were on Al substrates, are different interactions on the metal/oxide interface, which are dependent on the defect density and stoichiometry of the film.

Binding energy shifts and line shapes change considerably if carbon monoxide is adsorbed onto the metal deposits. The study of the CO adsorption is worthwhile, because extensive comparative material of CO adsorption on metal single crystals is available.[83, 173-175] The Pd 3d spectra with and without CO coverage for desposits at 90 K and 300 K are compared in Figure 24. If the available spectra are considered after CO saturated coverage at 90 K, the highest Pd coverage (corresponds to a mean island size of 70 Å) again shows clear parallels to the Pd(111) surface.[176-178] The Pd 3d signal of the clean surface shows a bulk and a surface component, which are shifted towards one another by about −0.3 eV[176] and which could not be resolved. CO adsorption leads to a shift of the surface component by about 1.1 eV to a higher binding energy; thus, both sections (see shoulder in spectrum) could be well separated. The bulk portion amounts to 40% in this case, decreases to 13% with 2 Å Pd (average island size of 22 Å), and can no longer be distinguished with 0.2 Å Pd (average island size 7.5 Å). The CO-induced binding energy shift grows with decreasing island size to about 1.5 eV. Experiments on single crystals show that the binding energy shifts depend on the number of coordinated CO molecules.[177, 178] Further analysis of the data[131] leads us to suspect that for smaller aggregates the number of coordinated CO molecules per surface Pd atom increases from one to two. The coordination numbers of transition metal carbonyls were never achieved.[131] Nevertheless, for cases in which the metal ionization in carbonyl compounds can be compared with those from the deposited particles,[179] the observed ionization energies of the carbonyl compounds are in agreement with those of the smallest aggregate. Figure 24b shows the comparison for Rh ionization. The binding energies obtained for the smallest aggregates are in agreement with the determined island sizes in the range of bi- to hexanuclear rhodium carbonyls.[179] The well-known $Rh(CO)_2$ species on an $Al_2O_3$ surface has an even higher binding energy of 310.2 eV.[179] However, the limited comparability of the substrate used must be taken into consideration in these comparisons.

Further indications of the electronic structure of the systems can be derived from the valence and the C 1s ionizations of the adsorbed CO and also from thermal desorption spectroscopy (TDS). The TD spectra of several Pd deposits are given in Figure 25.[140] For large Pd coverages, the desorption spectrum obtained closely resembles the spectrum of an adsorbate on a single crystal.[180] The relatively sharp, slightly intensive desorption maximum at 240 K stems from a hydrogen impurity.[131] As the size of the deposited particles decreases, a desorption maximum occurs between 250 and 300 K. The comparability of the system prepared at 90 K with the films produced at higher growth temperatures may be impaired by the limited thermal

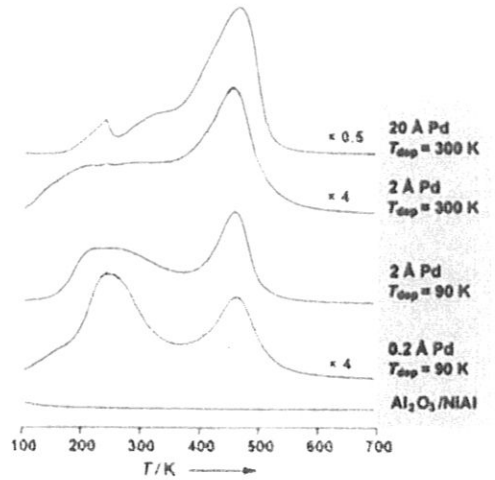


Figure 25. TD spectra of CO ($m/z$ = 28) for the $CO/Pd/Al_2O_3/NiAl(110)$ system (adsorption temperature 90 K, adsorbate quantity 20 L, heating rate about 1.5 $K s^{-1}$). The sequence of the TD spectra corresponds to increasing particle size from bottom to top. The deposited amounts are given in the form of effective layer thickness.

stability of the system. Thus, it is conceivable that the observed desorption between 200 and 300 K arises from a thermally limited structural reorganization of the metal aggregate alone as a result of the low growth temperature. A corresponding experiment based on warming the CO-saturated systems to 300 K and subsequent saturation with CO at 90 K, provides, however, a virtually identical desorption spectrum.[131] The low-temperature desorption in the range between 200 and 300 K is thus an inherent property of very small Pd aggregates.

The changes caused by CO adsorption in the region of the valence electron ionization are conveyed in Figure 26.[140] Firstly, the 4σ and 5σ/1π emissions of the chemisorbed CO are evident in the regions around 11 and 8 eV binding energy, respectively. The significantly higher intensity for the 90 K deposit compared to that of the film prepared at room temperature is easy to understand when the growth behavior is considered in terms of a clearly larger surface area in the first case.[131] The interaction of the valence states of the metal with those of the

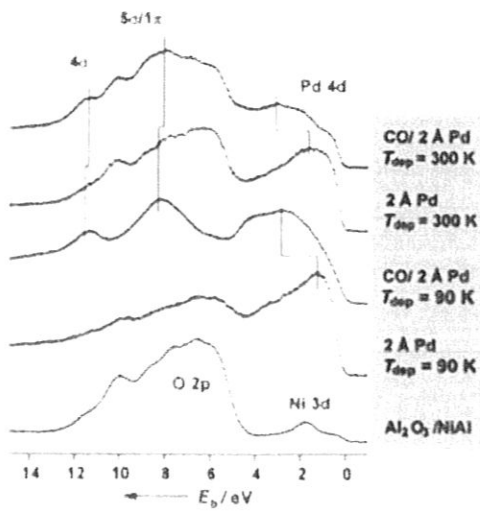


Figure 26. Comparison of the photoemission spectra of the valence electron ionizations of Pd deposits on $Al_2O_3/NiAl(110)$ before and after saturation with CO; $h\nu$ = 42 eV.

adsorbate leads to considerable changes in the region of Pd 4d emission. Here again, the considerable difference in size of the aggregate clearly shows the dependence on the conditions of preparation: owing to the low proportion of bulk atoms at small coverages, CO saturation for the 90 K deposit leads to even larger changes in the region of the Fermi level.

The C 1s spectra in Figure 27 are typical for molecularly bound CO and are therefore comparable to the spectra of transition metal carbonyls[181-183] and the C 1s spectrum of CO adsorbed on Pd (111).[184] The weakly defined fine structure in the latter spectrum is attributed to CO molecules on different adsorption sites. The C 1s spectrum for 12 Å Pd is, apart from insignificant broadening, identical to the spectrum of the single-crystal adsorbate. The transition to smaller aggregates reveals a significant shift to higher binding energies, an increase in the line width, and an increase in the intensity of "shake-up" satellites.[182,185-191] After the removal of some of the CO by warming to 300 K for a short period, a shift to lower binding energies as well as a decrease in line width, asymmetry, and shake-up intensity is observed (solid lines).

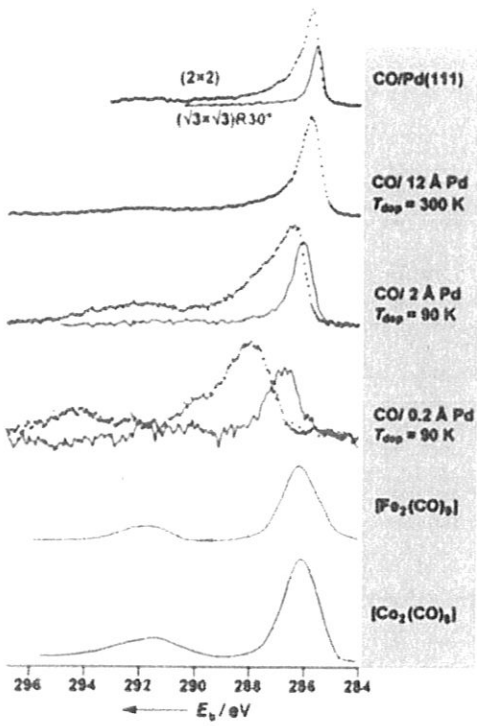


Figure 27. C 1s photoelectron spectra ($h\nu$ = 380 eV) of CO/Pd/$Al_2O_3$/NiAl(110) after CO saturation at 90 K (dotted line) as well as after a short warming to 300 K (solid line). For comparison, the C 1s spectra of two ordered CO superstructures on Pd(111) (top) as well as of two transition metal carbonyls (bottom) are given.

Shake-up satellites are a much-discussed and well-understood consequence of the fact that ionization is a complex multiparticle process, which despite the emission of a single electron leads to the simultaneous excitation of many ion states.[182,185-191] How intensive these different ion states appear in the spectrum of an adsorbate depends on, for example, how strong the bond is between CO and metal.[181,182,191] A detailed theoretical analysis shows that the charge transfer satellites adopt relatively large intensities for a weak chemisorption coupling between CO and metal.[181,182,191] Thus, in agreement with the results from TDS experiments, the changes of the satellite intensities confirm the occurrence of an important change that appears with decreasing particle size: while the strength of the chemisorption bond for small aggregates depends sensitively on the coverage, this is not so evident for large particles or single-crystal surfaces. The lack of well-ordered crystal surfaces for small aggregates leads inevitably to the situation that a distribution of different geometries can occur, which contribute decisively to the observed line broadening. Additional effects can also contribute to the line width,[189,192-194] but these shall not be discussed here.

The observed binding energy shift must, as when dealing with the Pd ionizations, be attributed to screening processes in the final state of the ionization.[163] This is verified by the X-ray absorption experiments[131] compiled in Figure 28. The result-

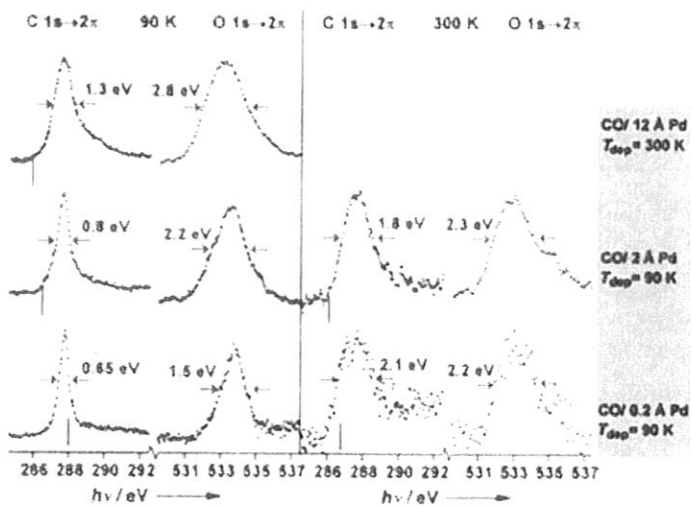


Figure 28. X-ray absorption spectra of C 1s and O 1s → 2π* resonances for CO/Pd/$Al_2O_3$/NiAl(110). Left: After CO saturation at 90 K. Right: After short warming to 300 K. The vertical marks show the position of the photoemission signals on a binding energy scale.

ing spectra show the excitation of a C 1s or an O 1s electron into the unfilled 2π orbital of the CO molecule.[195-199] Since the excited electron in the 2π orbital remains in the molecule, it is responsible for a large part of the core hole screening. Thus, whereas the screening and the associated shift in binding energy for the C 1s ionization is strongly dependent on the particle size, a much smaller influence on the signal is expected from the particle size itself with X-ray absorption. However, the strength of the bonding interaction between CO and metal should influence the signal in the following way: the synergic σ-donor-π-acceptor bonding mechanism leads to an interaction between unfilled CO π orbitals (see Figure 4) and filled Pd 4d orbitals. Since the 4d orbitals form a band, the interaction with the 2π orbitals of the CO molecule leads to a 2π state density distribution, whose width apart from the Pd 4d band width depends on the strength of the CO metal interaction. As systematic experiments on single-crystal adsorbates have shown, the lifetime of the excitation, vibrational excitations, and intermolecular interactions clearly play minimal roles.[199] Two effects dominate: the width of the resonance increases for systems with the same

geometry with increasing chemisorption energy, and it also increases with increasing coordination of the CO molecule; that is in the transition from atop to bridging to hollow site. These concepts can be used to interpret the resonance positions and widths in Figure 28.

While the ionization energy, indicated by the vertical markings in the C 1s → 2π spectrum, shifts to larger values as a function of the decreasing particle size, the C 1s → 2π resonance remains more or less at the same energy. At the same time with larger aggregates, it beomes broader, as expected for increasing chemisorption energy. The same is valid for the O 1s → 2π resonance in the case of the deposition at 90 K. After the sample is heated to 300 K, the resonance is broader, which is consistent with the discusssion conducted above—a clear indication of the strength of the bond! All experimental findings point to a strong chemisorption bond in the region of *small* CO coverage for the $Pd/Al_2O_3$ system *for all* island sizes. For small Pd aggregates the strength of this bond, however, decreases considerably for increasing coverage, and lies finally for the smallest Pd aggregate and CO-saturated coverage only in the region of weakly chemisorbed systems.

The comparison with Rh deposits is interesting. Thermal desorption and X-ray absorption spectroscopy of $Rh/Al_2O_3$ point to very modest changes of the CO-adsorption properties depending on the aggregate size. Thus, only the smallest islands exhibit a slightly different desorption behavior. A possible explanation for the different behavior of $Pd/Al_2O_3$ and $Rh/Al_2O_3$ could lie in the differences between the saturated-CO adsorption geometry of the smaller aggregates. It is known that on the relevant adsorption sites, Rh tends to an overall higher coordination through the adsorbate (formation of dicarbonyl species).[179] This is also in agreement with the results of experiments not considered here in detail,[200–203] according to which a reconstruction of the Rh islands—detectable by corresponding LEED profile measurements—takes place after CO exposure at 300 K, This, in turn, leads to an increased adsorption capacity after CO exposure at 90 K.[131]

### 4.4. Particle-Size-Dependent Reactivity

In contrast to the Pd deposits, the Rh deposits undergo a further reaction channel on warming,[104, 204–207] namely CO dissociation, which we will mention briefly in the following. This channel is active between 300 and 400 K, as shown in the spectra in Figure 29 a. The signal that verifies the appearance of atomic carbon occurs at 284 eV on warming. At the same time CO desorbs from the surface. After complete removal atomic carbon remains, and the 2π-CO resonance is no longer detectable in the X-ray absorption spectra.

The model systems offer the possibility of studying the dissociation as a function of particle size.[205–207] Figure 29 b shows a corresponding series of C 1s photoelectron spectra for Rh films deposited at 90 K that have an average layer thickness of between 0.6 and 12 Å and, thus, island sizes of between 5 and 30 Å. In each case the C 1s signals after CO saturation (40 L) at 90 K are compared with those obtained after a short warming to 400 or 600 K. If the relationship between the molecular C 1s emission immediately after the adsorption and the atomic C 1s signal after full CO desorption is considered for small and large aggregates, the latter signal is characterized by a considerably small relative intensity. Also a further quantitative analysis[131] leads to the conclusion (Figure 29b) that the smallest aggregate actually shows a low dissociation activity.[205–207] A geometric effect could play a role: the products of the dissociation process, atomic carbon and oxygen, prefer highly coordinated adsorption sites. Calculations[208] estimate that these sites have to be sufficiently apart from each other. A reaction path of this kind,

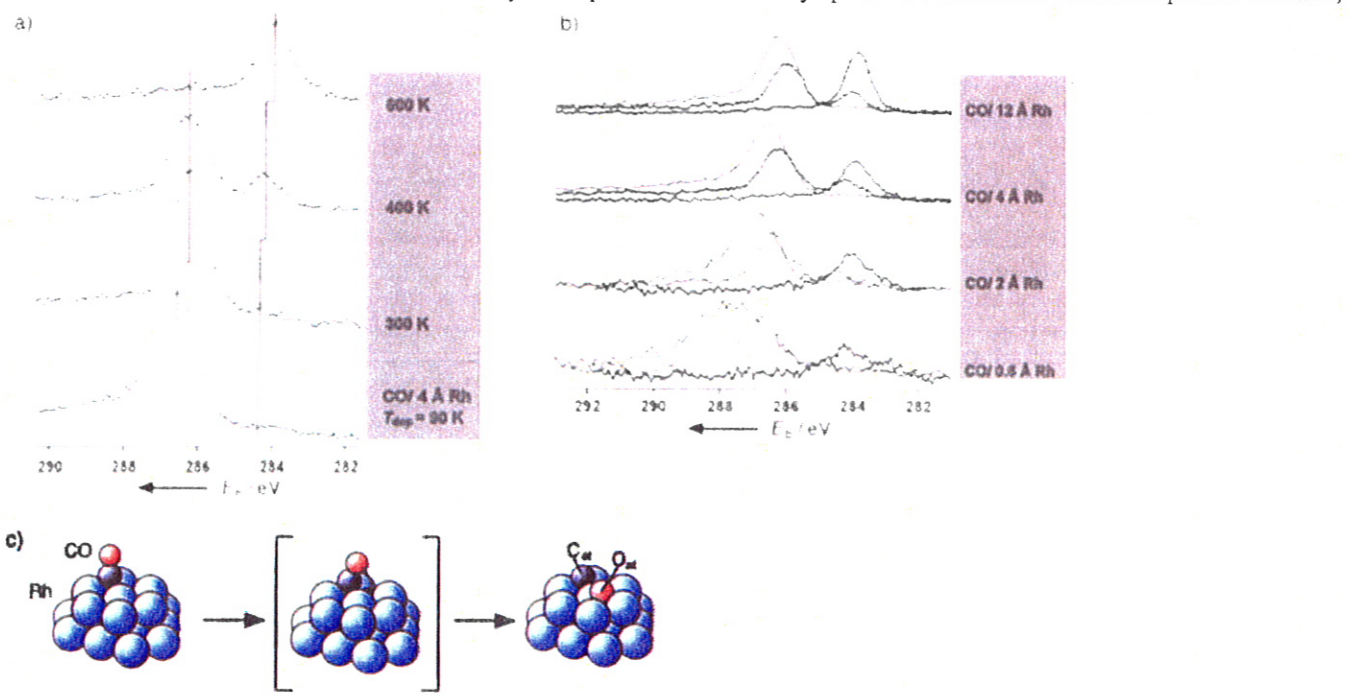


Figure 29. a) Series of C 1s photoelectron spectra ($h\nu$ = 380 eV) and C 1s → 2π* X-ray absorption spectra of $Rh/Al_2O_3/NiAl(110)$ after CO saturation at 90 K and short warming to the given temperatures. b) Comparison of the normalized C 1s photoelectron spectra ($h\nu$ = 380 eV) as a function of the thickness of the Rh layer after CO saturation at 90 K (solid line) as well as after warming to 400 K (dotted line) and 600 K. c) Schematic representation of the CO dissociation process.

as shown schematically in Figure 29c, implies that the Rh aggregates must have a considerable minimal size in order to permit efficient dissociation. In addition, electronic effects also play what may even be a dominant role.

We have arrived at a point in the discussion at which the reactivity could be linked with the particle morphology. In order to understand the effects that occur in catalyst preparation, attempts should next be made to influence[200–203] the morphology chemically and thereby control the chemical reactivity.

### 4.5. Influence of the Support Modification on the Morphology

In the context of the observations made in Section 4.1 about the modification of the aluminum oxide film by hydroxylation,[184–153] the effects the chemical modification has on the particle morphology will now be discussed briefly. This was investigated as part of a study, which included LEED, TDS, and photoelectron spectroscopic experiments.[131] Evidently, the interaction of Rh with the hydroxylated surface changed relative to that with the OH-free surface.[200–203] The Al 2p and O 1s photoelectron spectra, in particular, experienced changes through Rh deposition.[131] These changes are attributed to the occurrence of specific interactions between the deposited metal and the hydroxylated regions of the surface. In this way the formation of a highly dispersed Rh film results from the different interaction with the modified film at 300 K, which with regard to its growth behavior seems to be comparable with the metal films prepared on the unchanged oxide film at 90 K. This statement concerns merely the morphology; however, self-evidently a change in the Rh–substrate bond is expected. That this is in fact so becomes clear after CO exposure at 300 K. Unlike for the nonmodified substrate, in the case of the modified aluminum oxide film there is no reconstruction of the Rh islands under these conditions, which is evident from an enhancement of the CO adsorption ability.[131] This is consistent with a strong metal–substrate interaction. Finally, if the dissociation reactivity in the modified systems is considered, the activity is reduced to about half, which is consistent with the formation of smaller Rh aggregates on the modified film. In summary, the investigation of model systems allows the study of typical questions that arise with catalyst preparations, and, in particular, allows the changes that occur to be monitored directly by spectroscopy. The investigations are readily linked to the well-documented research on CO-induced Rh redispersion on $Al_2O_3$[200–203] and other substrates.[209–211] These investigations[200–203, 209–211] revealed that with sufficiently high CO partial pressures it is possible to reduce the metallic substrate under the formation of a dicarbonylrhodium species. This points to the fact that also in the real model systems carbonyl formation takes place with involvement of the hydroxyl groups of the $Al_2O_3$ surface.

### 4.6. Metal Deposition in Adsorbate Atmospheres

If the adsorbate is not applied separately but instead is present in the gas phase during the deposition, thus as a surfactant, it can intervene directly in the growth process.[212–215] An example is the deposition of Pd aggregates in a CO atmosphere.[136] Figure 30 shows the TD spectra after deposition of different amounts of Pd. The dominant feature in all of the spectra is a very sharp signal at 200 K. This is typical for the

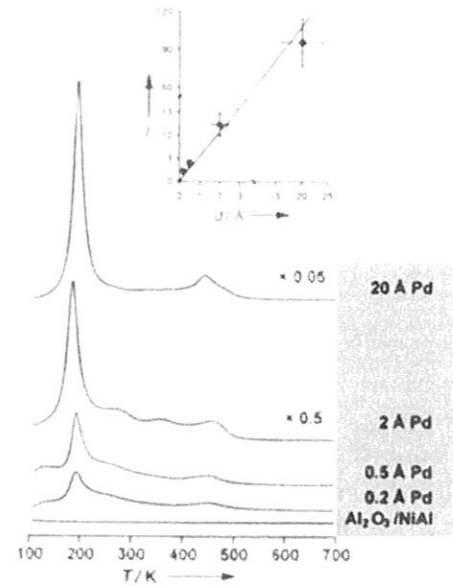


Figure 30. TD spectra of CO ($m/z = 28$) for different Pd coverages on $Al_2O_3$/NiAl(110), deposited in a CO atmosphere ($2 \times 10^{-6}$ mbar) at 90 K (heating rate about 1.5 K s$^{-1}$). The insert shows the integral intensity $I$ of the desorption signals as a function of the nominal Pd layer thickness $d$.

decomposition of a compound formed on the surface. The weak signals at higher temperatures (up to 500 K) are attributed to the desorption of intermediates, which form in the course of the decomposition. The intensity of the signal of the bond decomposition is directly proportional to the nominal layer thickness $d$, as shown in the insert in Figure 30. That this compound is a transition metal carbonyl is also confirmed by the valence photoelectron spectra and spectra of the inner electrons.[83, 181, 182]

Figure 31 a shows photoelectron spectra of the valence electrons that were obtained after stepwise Pd deposition in a CO atmosphere. Through the application of difference spectra, the substrate emission could be eliminated (Figure 31 b). It is now clear that, apart from a binding energy shift, the valence electron spectra are almost unchanged over the whole coverage range. At 20 Å Pd the spectra are dominated by the $1\pi/5\sigma$ emissions at 8.8 eV and the $4\sigma$ emissions at 11.9 eV,[83, 216] and, the ligand field splitting of the Pd 4d orbitals[181, 217] at 4.1 and 3.3 eV is clearly apparent. With sinking coverages the signals shift by about 1 eV to lower binding energies. A remarkable observation concerns the region of the Fermi energy ($E_b = 0$). Even with high coverages the state density remains minute in this region. Therefore, in agreement with the proposed formation of a metal carbonyl species, the presence of large metal aggregates can be excluded even at large coverages.

Schematically the growth of this metal carbonyl species can be conceived as shown in Figure 31 c. This model of the formation of branched, low-dimensional structures accounts for a variety of observations from LEED, XPS, and TDS experiments. The formation of this species is thoroughly unexpected,

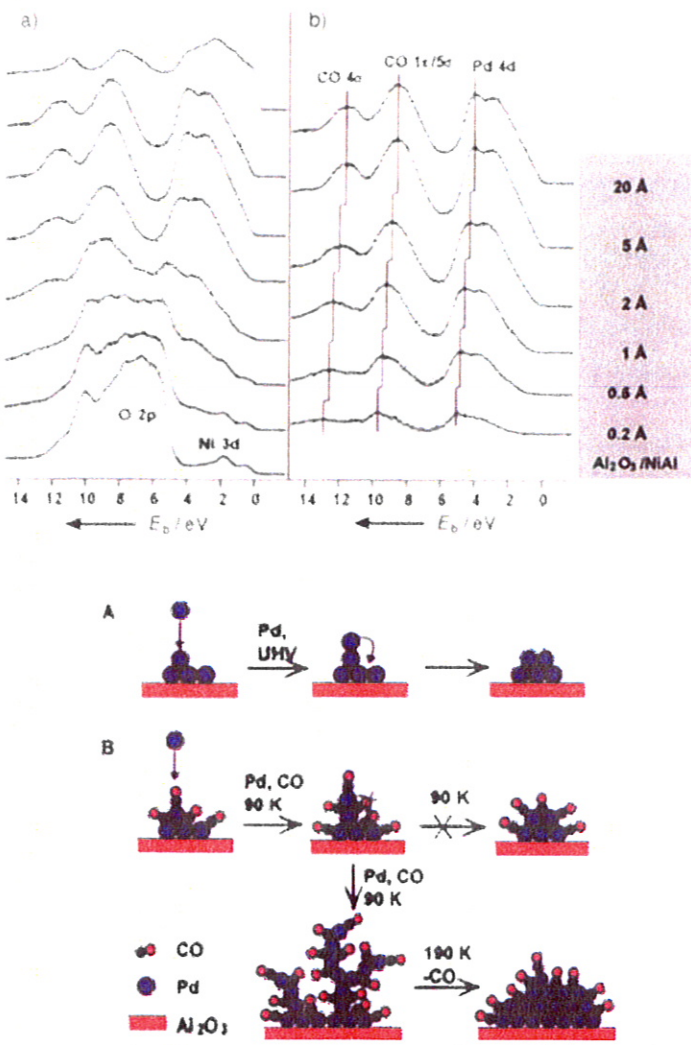


Figure 31. a) Valence electron–photoelectron spectra ($h\nu$ = 42 eV) after successive Pd deposits on $Al_2O_3$/NiAl(110) at 90 K in a CO atmosphere ($2 \times 10^{-6}$ mbar). The spectrum (top) for 20 Å Pd deposited under UHV conditions at 300 K and the ensuing CO saturation is given for comparison. b) Photoelectron difference spectra after subtraction of the oxide- and substrate-induced emissions. c) Schematic representation of a possible growth model for Pd deposition in a CO atmosphere.

since binary palladium carbonyls are generally very unstable.[217–224] Unlike for the $Pt/TiO_2$ system,[89] in which the CO-induced changes were discussed fundamentally on a thermodynamic basis, kinetic controlling mechanisms must be present here.

## 5. Synopsis

Today compound surfaces, such as those discussed here, can be prepared with different crystallographic orientations. The dependence of the chemical reactivity of the surface on the orientation can be clearly proven. This is substantiated by the presented comparison of nonpolar and polar surfaces of NiO and $Cr_2O_3$. The reactivity-accompanying restructuring for polar surfaces can be studied by electron diffraction and adsorption experiments. The adsorption behavior of small molecules on oxide surfaces has been investigated with a multitude of surface analytical techniques, and the adsorption sites as well as the adsorption geometry determined. Besides simple adsorption behavior, reactions that have a certain technical importance could also be investigated on single-crystal substrates, for example the DeNOx reaction and ethene polymerization. These reactions proceed on clean oxide surfaces. Furthermore, there is a range of reactions that are also of technical interest and that proceed on disperse metal systems on an oxide support. Such systems could, for example, be simulated on thin well-ordered $Al_2O_3$ layers by deposition of metals. The morphology and structure of the metal deposits can be studied by STM and LEED, and the adsorption of molecules on these complex systems by TDS and photoelectron spectroscopy. Here reactivity studies have provided clear indications about the particle-size-dependent reaction behavior, for example, for the CO dissociation on Rh.

Processes, which play a role in catalyst preparation and reaction, such as adsorbate-induced restructuring or increased influence of the metal dispersion by support modification, could be studied with the model systems. The models are also used to study metal deposition under ambient conditions. All in all the study on model compound surfaces should provide a number of interesting insights into the fundamental principles of catalytic reactions.

*A large number of co-workers obtained the results that are reported here. At the same time I have profited greatly through the collaboration and discussion with colleagues. I would like to mention several people in alphabetical order: B. Adam, Priv.-Doz. Dr. K. Al-Shamery, Prof. P. Andresen (Bielefeld), Dr. M. Bäumer, Dr. B. Bartos, Dr. B. Baumeister, Dr. I. Beauport, Dr. M. Beckendorf, M. Bender, Dr. D. Cappus, Dr. B. Dillmann, Dr. D. Ehrlich, Dr. C. Fischer, M. Frank, Dr. H. Geisler, Dr. H. Hamann, Dr. M. Hassel, Dr. I. Hemmerich, T. Hill, Dr. K. Homann, Dr. G. Illing, Dr. R. Jaeger, Dr. U. Katter, M. KLimenkov, Dr. J. Klinkmann, Dr. G. Klivenyi, T. Klüner, Priv.-Doz. Dr. H. Kuhlenbeck, Dr. J. Libuda, Dr. M. Menges, Dr. T. Mull, Prof. H. Neddermeyer (Halle), E. Neuhaus, Prof. M. Neumann (Osnabrück), Dr. G. Odörfer, Dr. T. Porwol, Dr. T. Risse, Dr. F. Rohr, Dr. A. Sandell, N. Sauerwald, H. Schlienz, O. Seiferth, Prof. V. Staemmler, S. Stempel, Dr. C. Ventrice, Dr. J. Wambach, M. Wilde, Dr. F. Winkelmann, K. Wirth, Dr. S. Wohlrab, Dr. C. Xu, Dr. I. Yakovkin (Kiev). I am also very grateful to a number of research development agencies for the support of our work: Deutsche Forschungsgemeinschaft, Ministerium für Wissenschaft und Forschung des Landes Nordrhein-Westfalen, Bundesministerium für Forschung und Technologie, European Union, German–Israeli Foundation and Fonds der Chemischen Industrie. At the same time I give my thanks to the Studienstiftung des Deutschen Volkes, which made available the grants for a number of my co-workers. Last but not least, I would like to thank the technical employees of Physikalische Chemie I of the Ruhr-Universität Bochum for their excellent support during the last nine years: H. Böhm, G. Humme, H. Messing, T. Michels, H. Rayess, C. Risse, U. Uhde, and T. Wasmuth.*

[1] G. Ertl, *Angew. Chem.* **1990**, *102*, 1258; *Angew. Chem. Int. Ed. Engl.* **1990**, *29*, 1219.
[2] G. Ertl, *Science*, **1991**, *254*, 1750.
[3] *Surface Science: The first 30 years*, North Holland, Amsterdam, **1994**.
[4] A. Zangwill, *Physics at Surfaces*, Cambridge University Press, Cambridge, **1988**.

[5] V. E. Henrich, P. A. Cox, *The Surface Science of Metal Oxides*, Cambridge University Press, Cambridge, 1994.
[6] C. Noguera, *Physics and Chemistry at Oxide Surfaces*, Cambridge University Press, Cambridge, 1996.
[7] "Adsorption on Ordered Surfaces of Ionic Solids and Thin Films": *Springer Ser. Surf. Sci.* 1993, *33*, 3–289
[8] C. Xu, D. W. Goodman in *Handbook of Heterogenous Catalysts* (Eds.: G. Ertl, H. Knözinger, J. Weitkamp), VCH, Weinheim, 1997, chapter 4.6.
[9] H.-J. Freund, *Ber. Bunsenges. Phys. Chem.* 1995, *99*, 1261.
[10] H.-J. Freund, H. Kuhlenbeck, V. Staemmler, *Rep. Progr. Phys.* 1996, *59*, 283.
[11] H.-J. Freund, *Phys. Status Solidi B* 1995, *192*, 407.
[12] H.-J. Freund, *NATO ASI Ser. Ser. C* 1996, *232*, 474.
[13] H. Kuhlenbeck, *Appl. Phys. A* 1994, *59*, 469.
[14] N. G. Condon, P. W. Murray, F. M. Leibsle, G. Thornton, A. R. Lennie, D. J. Vaughan, *Surf. Sci.* 1994, *310*, 260; A. R. Lennie, N. G. Condon, F. M. Leibsle, P. W. Murray, G. Thornton, D. J. Vaughan, *Phys. Rev. B* 1996, *53*, 10244.
[15] J.-W. He, P. J. Moller, *Chem. Phys. Lett.* 1986, 129; P. J. Moller in *Science of Ceramic Interfaces II*, (Ed.: J. Nowotny), 1994, p. 473.
[16] T. E. Madey, U. Diebold, J.-M. Pan, *Springer Ser. Surf. Sci.* 1993, *33*, 147.
[17] W. Weiss, A. Barbieri, M. A. van Hove, G. A. Somorjai, *Phys. Rev. Lett.* 1993, *71*, 1848; A. Barbieri, W. Weiss, M. A. van Hove, G. A. Somorjai, *Surf. Sci.* 1994, *302*, 259.
[18] D. Schmalzried, *Chemical Kinetics of Solids*, VCH, Weinheim, 1995.
[19] *Catalyst Supports and Supported Catalysts* (Ed.: A. B. Stiles) Butterworth, Boston, 1987.
[20] *Metal Clusters in Catalysis* (*Stud. Surf. Sci. Catal. B* 1986, *29*).
[21] M. Henzler, W. Göpel, *Oberflächenphysik des Festkörpers*, Teubner, Stuttgart, 1991.
[22] G. Ertl, J. Küppers, *Laser Energy Electrons and Surface Chemistry*, 2nd ed., VCH, Weinheim, 1985.
[23] H. Kuhlenbeck, G. Odörfer, R. Jäger, G. Illing, M. Menges, T. Mull, H.-J. Freund, M. Pöhlchen, V. Staemmler, S. Witzel, C. Scharfschwerdt, K. Wennemann, T. Liedtke, M. Neumann, *Phys. Rev. B* 1991, *43*, 1969.
[24] M. Haßel, H.-J. Freund, *Surf. Sci.* 1995, *325*, 163.
[25] D. Cappus, M. Haßel, E. Neuhaus, M. Heber, F. Rohr, H.-J. Freund, *Surf. Sci.* 1995, *337*, 268.
[26] P. W. Tasker, *J. Phys. C Solid State Phys.* 1979, *12*, 4977.
[27] J. W. Tasker, *Phil. Mag. A* 1979, *39*, 119.
[28] R. Lacman, *Colloq. Int. CNRS* 1965, *152*, 195.
[29] D. Wolf, *Phys. Rev. Lett.* 1992, *68*, 3315.
[30] A. Freitag, Dissertation, Ruhr-Universität Bochum, 1995.
[31] D. Cappus, X. Xu, D. Ehrlich, B. Dillmann, C. A. Ventrice, Jr., K. Al-Shamery, H. Kuhlenbeck, H.-J. Freund, *Chem. Phys.* 1993, *177*, 533.
[32] K. Refson, R. A. Wagelies, D. G. Fraser, M. C. Payne, M. H. Lee, V. Milan *Phys. Rev. B* 1995, *52*, 10833.
[33] C. G. Kinniburgh, *J. Phys. C Solid State Phys.* 1975, *8*, 2382.
[34] M. R. Welton-Cook, W. Berndt, *J. Phys. C Solid State Phys.* 1982, *15*, 5691.
[35] T. Urano, T. Kanaji, M. Kaburagi, *Surf. Sci.* 1983, *134*, 109.
[36] D. L. Blanchard, D. L. Lessor, J. P. LaFemina, D. R. Baer, W. K. Ford, T. Guo, *J. Vac. Sci. Technol. A* 1991, *9*, 1814.
[37] C. G. Kinniburgh, J. A. Walker, *Surf. Sci.* 1977, *63*, 274.
[38] R. C. Felton, M. Prutton, S. P. Tear, M. R. Welton-Cook, *Surf. Sci.* 1979, *88*, 474.
[39] K. H. Rieder, *Surf. Sci.* 1982, *148*, 37.
[40] R. Gerlach, A. Glebov, G. Lange, J. P. Toennies, H. Weiss, *Surf. Sci.* 1995, *331–333*, 2490.
[41] a) S. M. Vesecky, X. Xu, D. W. Goodman, *J. Vac. Sci. Technol. A* 1994, *12*, 2114; b) M. C. Wu, C. M. Truong, D. W. Goodman, *J. Phys. Chem.* 1993, *97*, 4182; c) C. M. Truong, M. C. Wu, D. W. Goodman, *J. Am. Soc.* 1993, *115*, 3647; d) J. W. He, J. S. Corneille, C. A. Estrada, M. C. Wu, D. W. Goodman, *J. Vac. Sci. Technol. A* 1992, *10*, 2248; e) M. C. Wu, C. A. Estrada, J. S. Corneille, D. W. Goodman, *J. Chem. Phys.* 1992, 96, 3892.
[42] J. Heidberg, D. Meine, *Ber. Bunsenges. Phys. Chem.* 1993, *97*, 211.
[43] A. Zecchina, D. Scarano, S. Bordiga, G. Ricchiardi, G. Spoto, F. Geobaldo, *Catal. Today*, 1996, *27*, 403.
[44] D. Cappus, J. Klinkmann, H. Kuhlenbeck, H.-J. Freund, *Surf. Sci. Lett.* 1995, *325*, L421.
[45] "Adsorption on Ordered Surfaces of Ionic Solids and Thin Films": G. Pacchioni, P. S. Bagus, *Springer Ser. Surf. Sci.* 1993, *33*, 180.
[46] a) K. M. Neyman, N. Rösch, *J. Chem. Phys.* 1992, *168*, 267; b) *Surf. Sci.* 1993, *297*, 223; c) *Chem. Phys.* 1993, *177*, 561;
[47] C. Pisani, R. Dovesi, R. Nada, S. Tamiro, *Surf. Sci.* 1989, *216*, 267.
[48] H.-J. Freund, M. Neumann, *Appl. Phys. A* 1988, *47*, 3.
[49] G. Pacchioni, G. Cogliandro, P. S. Bagus, *Surf. Sci.* 1991, *255*, 344; G. Pacchioni, P. S. Bagus, *NATO ASI Ser. Ser. B* 1992, *283*, 305.
[50] M. Pöhlchen, V. Staemmler, *J. Chem. Phys.* 1992, *97*, 2583.
[51] G. Blyholder, *J. Phys. Chem.* 1964, *68*, 2772.
[52] M. Schönnenbeck, D. Cappus, J. Klinkmann, H.-J. Freund, L. G. M. Pettersson, P. S. Bagus, *Surf. Sci.* 1996, *347*, 337.
[53] N. Floquet, I. C. Dufour, *Surf. Sci.* 1983, *126*, 543.
[54] V. E. Henrich, *Surf. Sci.* 1976, *57*, 385.
[55] H. Oniski, C. Egawa, T. Aruga, Y. Iwasawa, *Surf. Sci.* 1994, *310*, 135.
[56] C. R. Henry, H. Poppa, *Thin Sol. Films* 1990, *189*, 303.
[57] J. S. Foord, R. M. Lambert, *Surf. Sci.* 1986, *169*, 327.
[58] C. A. Ventrice Jr, H. Hannemann, A. Brodde, H. Neddermeyer, *Phys. Rev. B* 1994, *49*, 5773; H. Hannemann, C. A. Ventrice, T. Bertrams, A. Brodde, H. Neddermeyer *Phys. Stat. Sol. A* 1994, *146*, 289.
[59] F. Rohr, K. Wirth, J. Libuda, D. Cappus, M. Bäumer, H.-J. Freund, *Surf. Sci.* 1994, *315*, 1977.
[60] H. Kuhlenbeck, M. Frank, G. Lilienkamp, C. Koziol, T. Schmidt, E. Bauer, H.-J. Freund, unpublished results.
[61] H. Papp, B. Egersdörfer, unpublished results; B. Egersdörfer, Dissertation, Ruhr-Universität Bochum, 1993.
[62] H. Kuhlenbeck, C. Xu, B. Dillmann, M. Haßel, B. Adam, D. Ehrlich, S. Wohlrab, H.-J. Freund, U. A. Dittinger, H. Neddermeyer, M. Neuber, M. Neumann, *Ber. Bunsenges. Phys. Chem.* 1992, *96*, 15.
[63] C. A. Ventrice, D. Ehrlich, E. L. Garfunkel, B. Dillmann, D. Heskett, H.-J. Freund, *Phys. Rev. B* 1992, *46*, 12892.
[64] M. Bender, D. Ehrlich, I. N. Yakovkin, F. Rohr, M. Bäumer, H. Kuhlenbeck, H.-J. Freund, V. Staemmler, *J. Phys. Condens. Matter*, 1995, *7*, 5289.
[65] C. Xu, M. Haßel, H. Kuhlenbeck, H.-J. Freund, *Surf. Sci.* 1991, *258*, 23.
[66] C. Xu, B. Dillmann, H. Kuhlenbeck, H.-J. Freund, *Phys. Rev. Lett.* 1991, *67*, 3551.
[67] F. Rohr, M. Bäumer, H.-J. Freund, S. Müller, L. Hammer, K. Heinz, *Surf. Sci. Lett.* in press.
[68] M. Causa, C. Pisani, *Surf. Sci.* 1989, *215*, 271.
[69] F. Manassidin, A. Devita, M. Gillan, *Surf. Sci. Lett.* 1993, *285*, L517.
[70] B. Dillmann, O. Seiferth, G. Klivenyi, F. Rohr, I. Hemmerich, M. Bender, I. Yakovkin, D. Ehrlich, H.-J. Freund, *Faraday Disc. Chem. Soc.* in press.
[71] H.-J. Freund, B. Dillmann, O. Seiferth, G. Klivenyi, M. Bender, D. Ehrlich, I. Hemmerich, D. Cappus, *Catal. Today*, in press.
[72] B. Dillmann, Dissertation, Ruhr-Universität Bochum, 1996.
[73] I. Hemmerich, F. Rohr, O. Seiferth, B. Dillmann, H.-J. Freund, *Z. Phys. Chem.* in press.
[74] K. P. Huber, G. Herzberg, *Molecular Spectra and Molecular Structure, IV: Constants of Diatomic Molecules*, Van Nostrand Reinhold, New York, 1979.
[75] H. Ibach, D. L. Mills, *Electron Energy Loss Spectroscopy and Surface Vibrations*, Academic Press, New York, 1982.
[76] F. A. Miller, G. L. Carlton, W. B. White, *Spectrochim. Acta* 1959, *15*, 709; W. E. Hobbs, *J. Chem. Phys.* 1958, 28, 1220.
[77] P. J. M. Carrott, N. Sheppard, *J. Chem. Soc. Faraday Trans. 1* 1983, *79*, 2425.
[78] A. A. Davydor, Y. M. Shchekochikhin, N. P. Klier 1983, *79*, 2425; *Kinet. Katal.* 1992, *13*, 1888.
[79] I. E. Wachs, *Catal. Today*, in press.
[80] A. Zecchina, G. Spotoy, G. Ghiotti, *J. Mol. Catal.* 1992, *74*, 175.
[81] M. P. McDaniel, *Adv. Catal.* 1985, *33*, 47.
[82] D. D. Beck, J. H. Lunsford, *J. Catal.* 1981, *68*, 121; D. L. Myers, J. H. Lunsford, *ibid.* 1985, *92*, 260; *ibid.* 1986, 99.
[83] H.-J. Freund in *Handbook of Heterogenous Catalysis* (Eds.: G. Ertl, H. Knözinger, J. Weitkamp), 1997, part A, chapter 5.1, section 5.1.1.
[84] C. Xu, Dissertation, Ruhr-Universität Bochum, 1991.
[85] F. Rohr, Dissertation, Ruhr-Universität Bochum, 1996.
[86] S. K. Purnell, X. Xu, D. W. Goodman, B. C. Gates, *Langmuir* 1994, *10*, 3057; *J. Phys. Chem.* 1994, *98*, 4076.
[87] M. C. Wu, W. S. Oh, D. W. Goodman, *Surf. Sci.* 1995, *330*, 61.
[88] D. W. Goodman, *Chem. Rev.* 1995, *95*, 523; *Surf. Rev. Lett.* 1995, *2*, 9.
[89] H.-P. Steinrück, F. Pesty, L. Zhang, T. E. Madey, *Phys. Rev. B* 1995, *51*, 2427.
[90] M. C. Wu, P. J. Møller, *Surf. Sci.* 1989, *221*, 250.
[91] P. J. Møller, M. C. Wu, *Surf. Sci.* 1989, *224*, 265.
[92] M. C. Wu, P. J. Møller, *Surf. Sci.* 1990, *235*, 228.
[93] M. C. Wu, P. J. Møller in *The Structure of Surfaces III* (Eds.: S. Y. Tong, M. A. van Hove, K. Takayanaki, X. D. Xider), Springer, Berlin, 1991, p. 652.
[94] M. C. Wu, P. J. Møller, *Surf. Sci.* 1990, *250*, 179.
[95] Q. Guo, P. J. Møller, *Vacuum* 1990, *41*, 1114.
[96] P. J. Møller, Q. Guo, *Thin Sol. Films* 1991, *201*, 267.
[97] P. J. Møller, J. Nerlov, *Surf. Sci.* 1993, *307–309*, 591.
[98] O. Ge, P. J. Møller, *Appl. Surf. Sci.* 1994, *82–83*, 305.
[99] Q. Guo, P. J. Møller , *Surf. Sci. Lett.* in press.
[100] A. Ludviksson, K. H. Ernst, R. Zhang, C. T. Campbell, *J. Catal.* 1993, *141*, 380.
[101] K. H. Ernst, A. Ludviksson, R. Zhang, I. Yoshihara, C. T. Campbell, *Phys. Rev. B* 1993, *47*, 13782.
[102] E. I. Altman, R. J. Gorte, *Surf. Sci.* 1988, *195*, 392; *J. Catal.* 1988, *113*, 185.

[103] H. Cordatas, T. Bunlnesin, R. J. Gorte, *Surf. Sci.* **1995**, *323*, 219.
[104] E. I. Altman, R. J. Gorte, *Surf. Sci.* **1989**, *216*, 386.
[105] J.-M. Pan, B. L. Maschhoff, U. Diebold, T. E. Madey, *Surf. Sci.* **1993**, *291*, 381.
[106] U. Diebold, J.-M. Pan, T. E. Madey, *Phys. Rev. B* **1993**, *47*, 3868.
[107] J.-M. Pan, T. E. Madey, *J. Vac. Sci. Technol. A* **1993**, *11*, 1667.
[108] C. Duriez, C. R. Henry, C. Chapon, *Surf. Sci.* **1991**, 253, 190.
[109] C. R. Henry, C. Chapon, C. Duriez, S. Giorgio, *Surf. Sci.* **1991**, *253*, 177.
[110] C. R. Henry, C. Chapon, C. Goyhenex, R. Monot, *Surf. Sci.* **1992**, *272*, 283.
[111] C. Goyhenex, M. Meunier, C. R. Henry, *Surf. Sci.* **1996**, *350*, 103.
[112] C. Goyhenex, M. Croni, C. Claeys, C. R. Henry, *Surf. Sci.* **1996**, *352–354*, 475.
[113] P. Légaré, B. R. Bilwes, *Surf. Sci.* **1992**, *279*, 159.
[114] P. Légaré, F. Finck, R. Roche, G. Maire, *Z. Phys. D* **1989**, *12*, 19.
[115] E. Gillet, V. Matolin, *Z. Phys. D* **1991**, *19*, 361.
[116] B. Ealet, E. Gillet, *Surf. Sci.* **1993**, *281*, 91.
[117] S. Ogawa, S. Ichikawa, *Phys. Rev. B* **1995**, *51*, 17231.
[118] "Adsorption on Ordered Surfaces of Ionic Solids and Thin Films": M. Henzler, A. Stock, M. Böl, *Springer Ser. Surf. Sci.* **1993**, *33*, 15.
[119] K. M. Schröder, F. Schäfer, J. Wollschläger, M. Henzler, *Surf. Sci.* submitted.
[120] C. Schwennicke, J. Schimmelpfennig, H. Pfnür, *Surf. Sci.* **1993**, *293*, 57.
[121] R. M. Jaeger, H. Kuhlenbeck, H.-J. Freund, M. Wuttig, W. Hoffmann, R. Franchy, H. Ibach, *Surf. Sci.* **1991**, *259*, 235.
[122] M. Wuttig, W. Hoffmann, R. Jaeger, H. Kuhlenbeck, H.-J. Freund, *Mat. Res. Soc. Symp. Proc.* **1991**, *221*, 143.
[123] R. M. Jaeger, K. Homann, H. Kuhlenbeck, H.-J. Freund, *Chem. Phys. Lett.* **1993**, *203*, 41.
[124] R. M. Jaeger, J. Libuda, M. Bäumer, K. Homann, H. Kuhlenbeck, H.-J. Freund, *J. Electron Spectros. Relat. Phenom.* **1993**, *64/65*, 217.
[125] J. Libuda, M. Bäumer, H.-J. Freund, *J. Vac. Sci. Technol. A* **1994**, *12*, 2259.
[126] J. Libuda, F. Winkelmann, M. Bäumer, H.-J. Freund, T. Bertrams, H. Neddermeyer, K. Müller, *Surf. Sci.* **1994**, *318*, 61.
[127] P. J. Chen, D. W. Goodman, *Surf. Sci. Lett.* **1994**, *312*, L767.
[128] Y. Wu, H.-S. Tao, E. Garfunkel, T. E. Madey, N. D. Shinn, *Surf. Sci.* **1995**, *336*, 123.
[129] Y. Wu, E. Garfunkel, T. E. Madey, unpublished results.
[130] S. Stempel, Dissertation, Ruhr-Universität Bochum, in preparation.
[131] J. Libuda, Dissertation, Ruhr-Universität Bochum, **1996**.
[132] H.-J. Freund, B. Dillmann, D. Ehrlich, M. Haßel, R. M. Jaeger, H. Kuhlenbeck, C. A. Ventrice, F. Winkelmann, S. Wohlrab, C. Xu, Th. Bertrams, A. Brodde, H. Neddermeyer, *J. Mol. Catal.* **1993**, *82*, 143.
[133] F. Winkelmann, S. Wohlrab, J. Libuda, M. Bäumer, D. Cappus, M. Menges, K. Al-Shamery, H. Kuhlenbeck, H.- J. Freund, *Surf. Sci.* **1994**, *307–309*, 1148.
[134] S. Wohlrab, F. Winkelmann, J. Libuda, M. Bäumer, H. Kuhlenbeck, H.-J. Freund in *Surface Science Principles and Applications* (Eds.: R. J. MacDonald, E. C. Taglaner, K. Wandelt), Springer, Berlin, **1996**, pp. 193–202.
[135] T. Bertrams, F. Winkelmann, T. Uttich, H.-J. Freund, H. Neddermeyer, *Surf. Sci.* **1995**, *331–333*, 1515.
[136] J. Libuda, A. Sandell, M. Bäumer, H.-J. Freund, *Chem. Phys. Lett.* **1995**, *240*, 429.
[137] M. Bäumer, J. Libuda, A. Sandell, F. Winkelmann, H.-J. Freund, G. Graw, T. Bertrams, H. Neddermeyer, *Ber. Bunsenges. Phys. Chem.* **1995**, *99*, 1381.
[138] A. Sandell, J. Libuda, P. A. Brühwiler, S. Andersson, M. Bäumer, A. J. Maxwell, N. Martensson, H.-J. Freund, *J. Vac. Sci. Technol.*
[139] A. Sandell, J. Libuda, P. Brühwiler, S. Andersson, A. J. Maxwell, M. Bäumer, N. Martensson, H.-J. Freund, *J. Electron. Spectros. Relat. Phenom.* **1995**, *76*, 301.
[140] A. Sandell, J. Libuda, M. Bäumer, H.-J. Freund, *Surf. Sci.* **1996**, *346*, 108.
[141] "Elementary Processes in Excitations and Reactions on Solid Surfaces": J. Libuda, M. Frank, A. Sandell, S. Andersson, M. Bäumer, N. Martensson, H.-J. Freund, *Springer Ser. Solid State Sci.* **1996**, *121*, 210.
[142] A. Sandell, J. Libuda, P. A. Brühwiler, S. Andersson, M. Bäumer, A. J. Maxwell, N. Martensson, H.-J. Freund, *Phys. Rev. B*, in press.
[143] U. J. Katter, H. Schlienz, M. Beckendorf, H.-J. Freund, *Ber. Bunsenges. Phys. Chem.* **1993**, *97*, 340.
[144] B. Adam, Diplomarbeit, Ruhr-Universität Bochum, 1991.
[145] H. Isern, G. R. Castro, *Surf. Sci.* **1989**, *211/212*, 865.
[146] J. M. Mundenar, Dissertation, University of Pennsylvania, **1988**; R. H. Gaylord, Dissertation, University of Pennsylvania, **1987**.
[147] H. Pfnür, C. Schwennicke, J. Schimmelpfennig, *Springer Ser. Surf. Sci.* **1993**, *33*, 124.
[148] D. B. Almy, D. C. Foyt, J. M. White, *J. Electron Spectrosc. Relat. Phenom.* **1977**, *11*, 129.
[149] J. Paul, F. M. Hoffmann, *J. Phys. Chem.* **1986**, *21*, 5321.
[150] J. G. Chen, J. E. Crowell, J. T. Yates, Jr., *J. Phys. Chem.* **1986**, *84*, 5906.
[151] V. Coustet, J. Jupille, *Surf. Sci.* **1994**, *309*, 309; *Surf. Interface Anal.* **1994**, *22*, 280.
[152] B. G. Frederick, G. Apai, T. N. Rhodin, *Surf. Sci.* **1991**, *244*, 67.
[153] M. A. Schildbach, A. V. Hamza, *Surf. Sci.* **1993**, *282*, 306.
[154] J. Libuda, A. Sandell, P. Bruhweiler, M. Bäumer, H.-J. Freund, *Surf. Sci.* submitted.
[155] J. E. McDonald, J. G. Eberhart, *Trans. Met. Soc.* **1965**, AIME *233*, 512.
[156] D. Chatain, I. Rivollet, N. Eustathopoulos, *J. Chim. Phys.* **1986**, *83*, 561; *ibid.* **1987**, *84*, 201.
[157] E. Bauer, *Z. Kristallogr.* **1958**, *110*, 372.
[158] J. Wollschläger, J. Falta, M. Henzler, *Appl. Phys. A* **1990**, *50*, 57.
[159] P. R. Pukite, C. S. Lent, P. I. Cohen, *Surf. Sci.* **1985**, *161*, 39; C. S. Lent, P. I. Cohen, *ibid.* **1984**, *139*, 121.
[160] G. Beitel, K. Markert, J. Wiechers, J. Hrbek, R. J. Behm, *Springer Ser. Surf. Sci. 1993*, *33*, 7.
[161] A. F. Hollemann, E. Wiberg, *Lehrbuch der Anorganischen Chemie*, de Gruyter, Berlin, **1985**.
[162] M. G. Mason, *Phys. Rev. B* **1983**, *27*, 748.
[163] G. K. Wertheim, *Z. Phys. B* **1987**, *66*, 53.
[164] G. K. Wertheim, *Z. Phys. D* **1989**, *12*, 319.
[165] G. K. Wertheim, S. B. DiCenzo, D. N. E. Buchanan, *Phys. Rev. B* **1986**, *33*, 5384.
[166] F. A. Marks, I. Lindau, R. Browning, *J. Vac. Sci. Technol. A* **1990**, *8*, 3437.
[167] K. S. Schönhammer, O. Gunnarsson, *Z. Phys. B* **1978**, *30*, 297.
[168] K. Schönhammer, O. Gunnarsson, *Solid State Commun.* **1977**, *23*, 691.
[169] S. B. DiCenzo, G. K. Wertheim, *Commun. Solid State Phys.* **1985**, *11*, 203.
[170] S. Ogawa, S. Ichikawa, *Phys. Rev. B* **1995**, *51*, 17231.
[171] T. J. Sarapatka, *J. Phys. Chem.* **1993**, *97*, 11274.
[172] T. J. Sarapatka, *Chem. Phys. Lett.* **1993**, *212*, 37.
[173] *The Chemical Physics of Solid Surfaces and Heterogeneous Catalysis, Vol. 3, Chemisorption Systems, Part A*, (Eds.: D. A. King, D. P. Woodruff) Elsevier, Amsterdam, **1990**.
[174] "Applications of Synchrotron Radiation": N. Martensson, A. Nilsson, *Springer Ser. Surf. Sci.* **1995**, *35*, 65.
[175] H.-J. Freund, M. Neumann, *Appl. Phys. A* **1988**, *47*, 3.
[176] J. N. Andersen, D. Hennig, E. Lundgren, M. Methfessel, R. Nyholm, M. Scheffler, *Phys. Rev. B* **1994**, *50*, 17525.
[177] J. N. Andersen, M. Quarford, R. Nyholm, S. L. Sorensen, C. Wigren, *Phys. Rev. Lett.* **1991**, *67*, 2822.
[178] O. Björneholm, A. Nilsson, H. Tillborg, P. Bennich, A. Sandell, B. Hernnäs, C. Puglia, N. Martensson, *Surf. Sci.* **1994**, *315*, L983.
[179] B. G. Frederick, G. Apai, T. N. Rhodin, *J. Am. Chem. Soc.* **1987**, *109*, 4797.
[180] X. Guo, J. T. Yates, Jr., *J. Chem. Phys.* **1989**, *90*, 6761.
[181] E. W. Plummer, W. R. Salanek, J. S. Miller, Phys. *Rev. B* **1978**, *18*, 1673.
[182] H.-J. Freund, E. W. Plummer, *Phys. Rev. B* **1981**, *23*, 4859.
[183] H.-J. Freund, E. W. Plummer, W. R. Salaneck, R. W. Bigelow, *J. Chem. Phys* **1981**, *75*, 4275.
[184] J. N. Andersen, unveröffentlichte Ergebnisse.
[185] J. C. Fuggle, E. Umbach, D. Menzel, K. Brundle, *Solid State Commun.* **1978**, *27*, 65.
[186] K. Schönhammer, O. Gunnarsson, *Phys. Scr.* **1980**, *21*, 575.
[187] O. Gunnarsson, K. Schönhammer, *Phys. Rev. Lett.* **1978**, *41*, 1608.
[188] E. Umbach, *Surf. Sci.* **1982**, *117*, 482.
[189] A. Nilsson, N. Martensson, *Phys. Rev. B* **1989**, *40*, 10249.
[190] H. Tillborg, A. Nilsson, N. Martensson, *J. Electron Spectr. Relat. Phenom.* **1993**, *62*, 73.
[191] P. S. Bagus, M. Seel, *Phys. Rev. B* **1981**, *23*, 2065.
[192] A. Nilsson, N. Martensson, S. Svensson, L. Karlsson, D. Nordfors, U. Gelius, H. Ågren, *J. Chem. Phys.* **1992**, *96*, 8770.
[193] A. Sandell, J. Libuda, P. A. Brühwiler, S. Andersson, M. Bäumer, A. J. Maxwell, N. Martensson, H.-J. Freund, unpublished results.
[194] J. Bustad, C. Enkvist, S. Lunell, S. Svensson, *J. Electron Spectrosc. Relat. Phenom.* **1995**, *70*, 233.
[195] "NEXAFS Spectroscopy": J. Stöhr, *Springer Ser. Surf. Sci.* **1991**, *25*.
[196] U. von Barth, G. Grassmann, *Phys. Rev. B* **1982**, *25*, 5150.
[197] A. Nilsson, N. Martensson, *Physica B* **1995**, *209*, 19.
[198] A. Nilsson, O. Björneholm, E. O. F. Zdansky, H. Tillborg, N. Martensson, J. N. Andersen, R. Nyholm, *Chem. Phys. Lett.* **1992**, *197*, 12.
[199] O. Björneholm, A. Nilsson, E. O. F. Zdansky, A. Sandell, B. Hernnäs, H. Tillborg, J. N. Andersen, N. Martensson, *Phys. Rev. B* **1992**, *46*, 10353.
[200] H. F. J. van't Bilk, J. B. A. D. van Zon, T. Huizinga, J. C. Vis, D. C. Koningsberger, *J. Phys. Chem.* **1983**, *87*, 2264; *J. Am. Chem. Soc.* **1985**, *107*, 3139.
[201] F. Solymosi, M. Pásztor, *J. Phys. Chem.* **1985**, *89*, 4789.
[202] P. Basu, D. Panayotov, J. T. Yates, Jr., *J. Phys. Chem.* **1987**, *91*, 3133; *J. Am. Chem. Soc.* **1988**, *110*, 2074.
[203] F. Solymosi, H. Knözinger, *J. Chem. Soc. Faraday Trans.* **1990**, *86*, 389.
[204] D. N. Belton, S. J. Schmieg, *Surf. Sci.* **1988**, *202*, 238.
[205] V. Nehasil, I. Stará, V. Matolín, *Surf. Sci.* **1995**, *331–333*, 105.

[206] M. Rebholz, R. Prins, N. Kruse, *Surf. Sci.* **1991**, *259*, L797; *ibid.* **1992**, *269/270*, 293.
[207] V. Matolín, K. Mašek, M. H. Elyakhloufi, E. Gillet, *J. Catal.* **1993**, *143*, 492.
[208] A. de Koster, R. A. van Santen, *Surf. Sci.* **1990**, *233*, 366.
[209] A. Ludviksson, K. H. Ernst, R. Zhang, C. T. Campbell, *J. Catal.* **1993**, *141*, 380.
[210] N. Kruse, A. Gaussmann, *J. Catal.* **1993**, *144*, 525.
[211] M. H. El-yakhloufi, E. Gillet, *Catal. Lett.* **1993**, *17*, 11.
[212] H. A. van der Vegt, H. M. van Pinxteren, M. Lohmeier, E. Vlieg, J. M. C. Thornton, *Phys. Rev. Lett.* **1992**, *68*, 3335.
[213] M. Horn-von Hoegen, M. Pook, A. Al-Falou, B. H. MÜller, M. Henzler, *Surf. Sci.* **1993**, *284*, 53.
[214] H. Wolter, M. Schmidt, K. Wandelt, *Surf. Sci.* **1993**, *298*, 173.
[215] S. Esch, M. Hohage, T. Michely, G. Comsa, *Phys. Rev. Lett.* **1994**, *72*, 518.
[216] "Applications of Synchrotron Radiation": H.-J. Freund, H. Kuhlenbeck, *Springer Ser. Surf. Sci.* **1995**, *35*, 9.
[217] J. E. Reutt, L. S. Wang, Y. T. Lee, D. A. Shirley, *Chem. Phys. Lett.* **1986**, *126*, 399.
[218] J. H. Darling, J. S. Ogden, *Inorg. Chem.* **1972**, *11*, 666; *J. Chem. Soc. Dalton Trans.* **1972**, 2496.
[219] P. Kuendig, M. Moskovits, G. A. Ozin, *Can. J. Chem.* **1972**, *50*, 3587; *J. Mol. Struct.* **1972**, *14*, 137.
[220] H. Huber, P. Kuendig, M. Moskovits, G. A. Ozin, *Nature PS* **1972**, *235*, 98.
[221] L.-L. Sheu, H. Knözinger, W. M. H. Sachtler, *J. Am. Chem. Soc.* **1989**, *111*, 8125.
[222] Z. Zhang, H. Chen, W. M. H. Sachtler, *J. Chem. Soc. Faraday Trans.* **1991**, *87*, 1413.
[223] Z. Zhang, F. A. P. Cavalcanti, W. M. H. Sachtler, *Catal. Lett.* **1992**, *12*, 157.
[224] P. A. Hintz, K. M. Ervin, *J. Chem. Phys.* **1994**, *100*, 5715.